A Conformational Exploration of the Protonated and Unprotonated Macrolide Antibiotic Roxithromycin: Comparative Study by Molecular Dynamics and NMR Spectroscopy in Solution

Josyane Gharbi-Benarous, Patrick Ladam, Marcel Delaforge and Jean-Pierre Girault*
Université René Descartes, Laboratoire de Chimie et Biochimie Pharmacologiques et Toxicologiques, CNRS URA 400, 45 rue des Saint-Pères, F-75270 Paris Cedex 06, France

Molecular dynamics simulations (MD) have been performed on protonated and unprotonated roxithromycin, a novel macrolide antibiotic, using the crystallographic coordinates as the starting conformation in order to understand conformational changes. In all cases the 100 ps time scale seemed adequate for sampling an ensemble of solution conformers. Roxithromycin did not unfold appreciably during a 100 ps simulation while, for the protonated form, the desosamine unit underwent an interesting conformational reorganization ('**a** $\Longleftrightarrow$ **c**') during its evolution from the crystal structure form. MD indicate insignificant folding relative to the C(3)–C(5) region and it is believed that the necessary activation energy for this observed transitional event ('**A** $\Longleftrightarrow$ **B**') is probably not attained in solution, in contrast with erythromycin A. Long-range ^{13}C–^{1}H coupling constants are reported and correlated to the glycosidic torsional angles. The use of MD simulation has facilitated the confirmation of solution conformation as predicted by NMR spectroscopy. Moreover, it gives structural information on the different conformers present in solution. The data are not compatible with the conformation observed in the crystal structure only, and support a single conformation model **Aa** for roxithromycin with two types of hydrogen bonding (**II** and **III**). However, conformational averaging of **Aa** and **Ac** can give good agreement between theoretical and experimental data for the protonated analogue. The different values of potential energies for the observed low-energy conformers support the importance of hydrogen bonding in macrolide conformation. It appears that intra-residue hydrogen bonding, such as type **III**, 11-OH///O=C (1), plays a role in determining the conformation of a large region [from C(9) to C(1)] of the antibiotic macrolide. Roxithromycin probably exists in the form of two ring-conformers '**AII** $\Longleftrightarrow$ **AIII**' and, in $CDCl_3$, a hydrogen bridge is formed that lowers the barrier enough to make interconversion possible.

Some macrolide antibiotics derived from erythromycin A have been implicated in numerous drug interactions. In fact, these macrolides antibiotics have been shown to affect cytochrome P-450. They lead to the induction of cytochrome P-450 and to a stable metabolite–cytochrome P-450 complex after oxidation of their dimethylamino function. Recently a new antibiotic, roxithromycin has been put on the market; it is derived from erythromycin A, the 9-keto group being replaced by a 9-[*O*-(2,5-dioxahexyl)oxime] chain.[1]

It should be noted that tautomeric forms of erythromycin A have been implicated in certain biological reactions of this molecule.[2] This type of tautomerism is not observed for 9-oximo derivatives[3] such as roxithromycin.

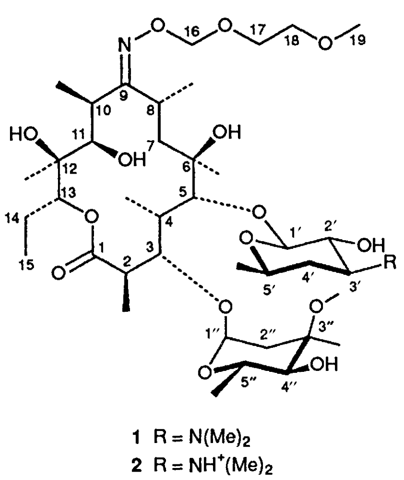

1 R = N(Me)$_2$
2 R = NH$^+$(Me)$_2$

This new antibiotic retains the antibacterial activity of erythromycin A but, unlike erythromycin A, roxithromycin does not form an inhibitory P-450–metabolite complex *in vivo*, even at high doses (1 g kg^{-1}) and does not induce hepatic cytochrome P-450. These properties are in good agreement with the absence of metabolic drug interaction observed after roxithromycin treatments.[4–7] *In vitro*, roxithromycin has little affinity for the cytochrome P-450 binding site, and it is unable to form significant quantities of P-450–metabolite complex.[7]

A preliminary communication on roxithromycin, compound **1**, has been published[8] and the solution conformation of roxithromycin and its motional properties have also been studied by NMR spectroscopy. It can be concluded that the major conformation of this compound existing in solution is very similar to that in the solid state. The observed structure confirmed the tendency of the desosamine sugar to adopt a conformation with an orientation nearly perpendicular to the macrocyclic lactone ring. In the solid state the chain is bound by an intramolecular hydrogen bond 19-OMe to 6-OH which is certainly thought to occur in solution. The NOE information has shown that the oxime chain is directed towards the 6-OH group, the end being close to the cladinose sugar, which is thus pushed back onto the desosamine ring.

In all solvents tested a minor component was present. Its structure elucidation by NMR however, was expected to be complex (because it can only be investigated as the minor component present in a mixture with the major ones) and would at least require a conformational analysis of the macrolide ring. Everett and Tyler proposed two diamond lattice conformation models **A** and **B** for the aglycones of the 14-membered

Table 1 Torsion angles φ (°) around the erythronolide ring for the crystal structures of roxithromycin [15] and erythromycylamine derivatives [10] and for *minimized* structures derived from MD calculations of roxithromycin (**1**) and protonated roxithromycin (**2**) at 300 K

	MD structures[a]					X-ray structures		
	Roxithromycin		Protonated Roxithromycin			'folded-out'[b]	'folded-in'[c]	
φ	**Aa**	**Bb**	**Aa**	**Ac**	**Bb**[d]	**A**	**B′**	**B**
O(14)–C(1)–C(2)–C(3)	116.8	113.4	116.7	114.6	109.3[d]	121.2	79.9	94.4
C(1)–C(2)–C(3)–C(4)	−75.8	−113.1	−75.2	−71.5	−121.4[d]	−69.6	−130.8	−129.6
C(2)–C(3)–C(4)–C(5)	160.5	164.9	160.4	159.7	166.7	163.4	173.6	172.8
C(3)–C(4)–C(5)–C(6)	*−95.6*	*−86.0*	*−95.7*	*−93.7*	*−78.6*	*−106.9*	*−100.1*	*−116.9*
C(4)–C(5)–C(6)–C(7)	−77.8	−65.8	−77.9	−81.4	−65.0[d]	−72.0	60.1	67.6
C(5)–C(6)–C(7)–C(8)	178.0	176.7	177.9	177.2	177.7	174.7	148.0[e]	55.5[e]
C(6)–C(7)–C(8)–C(9)	−69.0	−65.1	−69	−69.2	−67.8[d]	−75.5	178.9	177.4
C(7)–C(8)–C(9)–C(10)	−66.2	−74.8	−66.4	−65.2	−74.6	−63.3	−53.9[e]	34.5[e]
C(8)–C(9)–C(10)–C(11)	113.1	114.5	113.2	114.1	114.0[d]	123.7	97.2	70.3
C(9)–C(10)–C(11)–C(12)	−168.4	−170.4	−168.0	−167.5	−170.8	−166.2	−164.0	−156.0
C(10)–C(11)–C(12)–C(13)	170.0	168.3	170.1	170.2	168.2	164.2	165.6	173.6
C(11)–C(12)–C(13)–O(14)	−69.9	−69.2	−70.0	−70.2	−68.7	−82	−70.1	−59.5
C(12)–C(13)–O(14)–C(1)	111.1	127.0	110.6	108.7	129.4[d]	114.4	144.6	156.0
C(13)–O(14)–C(1)–C(2)	172.4	−172.8	172.2	171.6	−169.9[d]	172.9	−177.9	−173.6

[a] These values are given by molecular dynamics in five different conformations minimized at 12 and 65 ps (**BbI**, **AaII**) for roxithromycin (**1**) and at 67, 78 and 90 ps (**AaII**, **AcII**, **BbI**) for protonated roxithromycin (**2**). [b] The 'folded-out' type, conformation **A**, is found for the crystal structure of roxithromycin (its name '**A**' is based on the crystal structure of erythromycin A).[15] [c] X-ray data [10] of an erythromycylamine derivative: (9*S*,22*R*)-9,11-*N*,*O*-(2-methoxyethoxyethylidene)erythromycylamine A in the corresponding C(3) to C(5) 'folded-in' conformation type **B**. The 'folded-in' conformation **B′** is based on the crystal structure of an erythromycin derivative: (*E*)-11-*O*-(2-dimethylaminoethoxy)methyl-9-deoxy-9-methoxyiminoerythromycin A. [d] These two minimized conformations **Bb** (12 ps and 90 ps) differ from conformations **B** and **B′** mainly in the C(5) to C(10) region while the dihedral angles around C(2)C(3) and C(13)–O(14)–C(1) rotate to about the same value. The relative orientation of the sugar rings depends on the rotation, principally about C(4)–C(5) bond corresponding to the dihedral angles (in italics). [e] Conformations **B** and **B′** differ from each other mainly in the C(6) to C(9) portions of the lactone ring [C(5)–C(6)–C(7)–C(8) = 148.0°, C(7)–C(8)–C(9)–C(10) = −53.9° in the conformation type **B′**].

macrolides.[9] Extensive NMR work [10] has shown that for erythromycin A and some of its C(9) derivatives in $CDCl_3$, their macrocyclic lactone rings are in fast exchange between two types of conformation—the C(3)–C(5) 'folded-out' type (conformation **A**) and the corresponding C(3)–C(5) 'folded-in' type (conformation **B** or **B′**). The conformational equilibria were originally described as involving conformations **A** and **B**, but without flexibility in the C(6)–C(9) region. However, the **B′** conformation was subsequently identified and should be included in the conformational equilibria of these compounds (Table 1).

On the other hand, a structure **S** has recently been detected in a crystal structure of a 9-dihydroerythronolide B derivative,[11] in which 11-OH may form a hydrogen bond bridge to the carbonyl oxygen of the C(1)=O group. One difference lies in the dihedral angle C(6)–C(7)–C(8)–C(9) which, owing to ring effects, is reduced to *ca.* 60° [O(11) and C(1)=O are close enough to form a hydrogen bridge]. It is concluded that **A** and **S** probably exist in the form of two ring-conformers in $CDCl_3$ solution.

Because of these observations, and a report that the crystal structure conformation cannot account for all the NMR data,[8] we decided that further study was needed. We hoped to carry out a systematic search for the lactone conformation by performing molecular-mechanics calculations. The conformational analysis of the macrolide will be difficult in this case, as similar conformations in solution and hence similar corresponding NMR spectra would be expected, since both conformers differ only in the flexibility of the three units (macrocycle, oxime chain and particularly desosamine sugar). The combination of NMR analysis with molecular dynamics and mechanics calculations led us to a complete assignment of each conformer and the conformation of the molecules in solution. Since no explicit solvent molecules were incorporated during the run, the relative permittivity was set up as distance dependent ($\varepsilon = R_{ij}$), in order to mimic the solvent effect.[12]

Apart from the flexibility of the different units, another feature under investigation by modelling is the persistence in solution of the hydrogen bonds found in the crystal. Recently it was considered that the octanol–water partitition coefficient of 408 for roxithromycin could hardly account for the higher lipid solubility and hence the better permeability of roxithromycin through some tissues.[13]

An extension of our work [14] was to compare roxithromycin and erythromycin A, which show different biological effects, and we studied the correlation between the conformation and the biological properties. Our results demonstrated the importance of the orientation of the ether chain and of the sugar rings with respect to one another and to the lactone ring. We argued, supported by detailed ^{13}C T_1 and NOE measurements, that, for roxithromycin, the hydroxy protons 6-OH and 11-OH are implicated in hydrogen bonding with the oxime chain. Thus the resulting hydrophobicity and globular structure of roxithromycin with respect to erythromycin A and the effect of the pH, could be related to its biological properties.

Indeed, the presence of protonated roxithromycin at physiological pH has consequences for their relative ease of access to the hydrophobic active site of cytochrome P-450 and roxithromycin is only metabolized into a complex absorbing at 455 nm at pH 8 or higher. However, the protonated roxithromycin, compound **2**, has NMR parameters very similar to those for the unprotonated form **1**, which renders their respective spectra practically identical. Only in 'commercial' $CDCl_3$, which is often acidic and wet, when the concentration of roxithromycin is decreased, did we observe an important shift of the initial *N*,*N*-dimethylamino signal, a singlet at 2.29 ppm ($c = 10^{-2}$ mol dm^{-3}), towards its final position, two doublets due to non-equivalent methyl groups in the protonated form, at 2.81 and 2.94 ppm ($c = 10^{-3}$ mol dm^{-3}), similar to the signal corresponding to the protonated form obtained at pH 3 (in D_2O).

The important question arises of whether structural differences are relevant to corresponding differences in function. The different biological activity observed in the formation of a

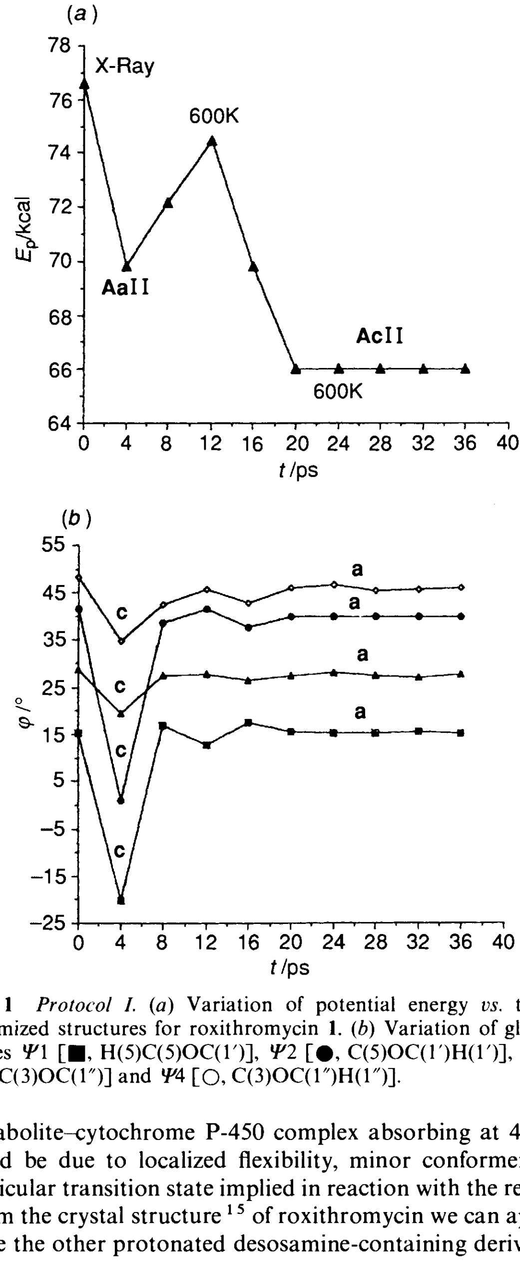

Fig. 1 *Protocol I.* (*a*) Variation of potential energy *vs.* time for minimized structures for roxithromycin **1**. (*b*) Variation of glycosidic angles Ψ1 [■, H(5)C(5)OC(1′)], Ψ2 [●, C(5)OC(1′)H(1′)], Ψ3 [▲, H(3)C(3)OC(1″)] and Ψ4 [○, C(3)OC(1″)H(1″)].

metabolite–cytochrome P-450 complex absorbing at 455 nm, could be due to localized flexibility, minor conformers or a particular transition state implied in reaction with the receptor. From the crystal structure [15] of roxithromycin we can approximate the other protonated desosamine-containing derivative **2** and perform a simulation to determine any differences in the presence and absence of an NH^+ ion.

Although MD can be used to generate potential solution structures, one difficulty is that it is not always clear how long a given MD simulation should be performed with respect to the time scale of observable conformational events, in order to conclude whether a reasonable solution structure has been attained.

Here we will describe in detail the modelling procedure, providing further support for the conformational study of various macrolide derivatives with different biological activities. The different protocols used for the MD simulations, could be used to generate many different structures and to explore fully the conformational space of these compounds.

Results and Discussion

We report on the conformational analysis of roxithromycin **1** and protonated roxithromycin **2** by computational chemical methods (molecular-dynamics and molecular-mechanics calculations), X-ray analysis (Table 1) and NMR spectroscopy in solution (Tables 2 and 3).

In order to obtain more detailed structures, and conformations which are in better agreement with the NMR data, we performed the molecular-dynamics calculations starting with the X-ray crystal structure,[15] without applying interproton distances or dihedral angle constraints (a systematic search is valid only for small molecules). The final structures obtained after several such calculations were examined for the *overall* energetic favourability and compared with the structure derived from the NMR data. Table 2 compares the NMR data with the resulting dihedral angles for all different conformations obtained from MD. The similarity between the geometry in solution and several MD conformers was also investigated by the intensive NOESY correlations observed (Table 3).

In Table 4 we report the amplitude, the average and the predominant values of endocyclic torsion angles and in the same manner, in Table 5, vicinal proton and some heteronuclear $^{1}H-^{13}C$ dihedral angles for the macrocycle, for the 100 minimized structures generated. They illustrate the final conformations (100 ps) of both **1** and **2** and the corresponding initial ones (0 ps).

The different conformations of the macrocyclic lactone ring, the sugar moieties and the oxime chain with their characteristics (dihedral angles, spatial proximities, hydrogen bonding and potential energy for each conformation type) and with their statistical participation (%) are reported in Tables 6 and 7 for roxithromycin **1** and protonated roxithromycin **2**, respectively. These data will later be compared with those found by NMR spectroscopy in solution. All the notation for conformer designation is defined in Table 8, *i.e.* **A**, **B**, **a**, **b**, **c**, **d**, **I**, **II**, **III**.

Molecular Dynamics and Energy Minimization.—A molecular dynamics simulation was performed for roxithromycin **1** and protonated roxithromycin **2** using the 'DISCOVER' program of Biosym package with the CVFF forcefield from Dauber–Osguthorpe and Hagler [16] on a Silicon-Graphics 4D-20G computer.

The DISCOVER program system [16] was used for the molecular dynamics optimization of the structures in the following manner. The starting coordinates of **1** and **2** were taken from the X-ray crystal structure of roxithromycin, with the desosamine sugar modified to include a protonated amino group for **2**. The ionization state of the dimethylamino group of the desosamine sugar was taken into account [17] in order to check the eventual consequences on conformational properties according to the electrostatic term.

Prior to this a run was performed in which the structure was energy minimized. During a subsequent 4 ps equilibration period the system was coupled to a thermal bath [18] at 300 K.

Protocol I (Fig. 1). For a preliminary conformational exploration, we performed for **1** a 40 ps MD run with temperature jumps. After energy minimization and an equilibration period, the simulation was then continued for a 8 ps period at 300 K, followed by a temperature jump to 600 K for 4 ps. This alternation was repeated until a total simulation time of 40 ps was reached. The simulation was stopped every 4 ps and the structure was energy minimized using the previously described method. The short periods at 600 K were incorporated in order to prevent staying in the same local energy gap and to help the jump over eventual barriers by increasing the kinetic energy to identify the global energy minimum.

The initial conformation tested is 10 kcal* higher than the minimum and starts from the X-ray crystal structure. In practice it does not contribute measurably but it is a basic conformation involving a macrocycle conformation **A**, a sugar ring orientation **a** and a type **I** hydrogen bond [6-OH///O(16); 12-OH///OH-11; 4″-OH///OMe-3″].

The first energy minimum of this molecule (above 3 kcal per

* 1 cal = 4.184 J.

Table 2 Dihedral angles φ (°) and corresponding coupling constants (^3J/Hz) for roxithromycin (**1**)

Vicinal pair	φX-Ray[15]	$^3J_{calc}$[a]	$^3J_{exp}$	φ_{exp}	φMD[b] **AaII**	**BbI**	**AcII**
J_{HH}							
2-H, 3-H	170.5	11.1	9.9	160	159	117	165
3-H, 4-H	−71.5	2.4	1.5	−72	−73	−70	−74
4-H, 5-H	129.6	5.9	7.4	137	136	146	138.5
7_{ax}-H, 8-H	164.0	11.9	10.5	154	178	179	178
7_{eq}-H, 8-H	76	2.0	3.5	60	−69	−67	−69
10-H, 11-H	70.8	2.4	2.1	60	66	66	67
13-H, 14_{ax}-H	171.8	11.7	11.2	168	174	175	175
13-H, 14_{eq}-H	68.5	2.4	2.5	65	69	70	69
$1'_{ax}$-H, $2'_{ax}$-H	175.0	9.8	7.5	171	174	173	173
$2'_{ax}$-H, $3'_{ax}$-H	176.3	11.1	10.5	174	180	179	179
$3'_{ax}$-H, $4'_{ax}$-H	−177.9	12.3	11.2	−169	−179	180	180
$4'_{ax}$-H, $5'_{ax}$-H	176.7	12.1	10.8	172	−175	−173	−173
$1''_{eq}$-H, $2''_{eq}$-H	72.6	2.2	1.7	72.6	69	72	72
$4''_{ax}$-H, $5''_{ax}$-H	178.6	10.8	9.5	178.6	174	174	174
J_{CH}							
Macrocycle							
3-H, 1-C	50	2.5	3.3	41	41	2.5	46
5-H, 3-C	13	5.3	4.8	23	19	30	22
5-H, 6-C_{Me}	44	3	2.5	49	43	55	46
13-H, 1-C	−3.5	5.6	3.5	38	−8	10	−10
13-H, 11-C	36.7	3.7	s	*c*	51	52	53
13-H, 15-C_{Me}	−49.8	2.5	s	*c*	−52	−53	−52
Glycosidic bonds							
5-H, 1′-C	14.3	5.3	5.3	14	16	16	−27
5-C, 1′-H	46.0	2.8	4.5	28	39	51	8
3-H, 1″-C	28.2	4.4	5.3	14	27	35	22
3-C, 1″-H	43.0	3.1	s	*c*	46	43	39

[a] The calculated $^3J_{HH}$ values for the solid-state conformation would be estimated by a Karplus equation of the following type:[8,21] $^3J_{HH} = (7.8 - \cos\varphi + 5.6\cos 2\varphi)(1 - n\Sigma\Delta Ex_i)$ and all $^3J_{CH}$ values by a Karplus-type equation of the form:[20] $^3J_{CH} = 5.7\cos^2\varphi - 0.6\cos\varphi + 0.5$. [b] These values are given by molecular dynamics in three different conformations minimized at 12 and 65 ps (**AaII**, **BbI**) for roxithromycin and at 78 ps (**AcII**) for protonated roxithromycin. [c] These signals are detected as singlets (they cannot be correctly estimated because of low resolution) when $^3J_{CH}$ coupling constants are <2 Hz and the corresponding dihedral angles are $50 > \varphi > 120°$ (±).

minimum) reveals a small amount of new information about the rotation of the desosamine sugar. The greatest discrepancy between the crystal structure and the observed conformer occurs for the glycosidic and two macrocyclic dihedral angles: Ψ1, H(5)–C(5)–O(5)–C(1′) ($\Delta = -35.5°$); Ψ2, C(5)–O(5)–C(1′)–H(1′) ($\Delta = -40.5°$); Ψ3, H(3)–C(3)–O(3)–C(1″) ($\Delta = -9.3°$); Ψ4, C(3)–O(3)–C(1″)–H(1″) ($\Delta = -13.4°$); H(4)–C(4)–C(5)–H(5) ($\Delta = +12°$); H(5)–C(5)–C(6)–C(6-Me) ($\Delta = -6°$). This conformation shows the same rigid macrocycle conformation **A**, but with a planar desosamine ring **c** and a type **II** hydrogen bonding [6-OH///O(17); 12-OH///OH-11; 4″- OH/// OMe-3″], and is designated the **AcII** structure (Fig. 2).

Finally, the energy minimum structure is very similar to that predicted by NMR spectroscopy in solution, namely conformation **AaII** (Fig. 2). If we compare the resulting coupling constants with the NMR data (Table 2), we observe slight variations: (Δ in Hz) H(2)H(3) (−0.2); H(4)H(5) (−0.3); H(5)C(6-Me) (−0.5); Ψ1 (+0.1); Ψ2 (+1); Ψ3 (+1); Ψ4 (+0.3). As seen from the NMR data, the oxime chain is anchored to the erythronolide by the 6-OH group and the close approach of of 19-OMe and H(3), as observed by NOE (Table 3), is then confirmed.

Protocol II (Fig. 3). In order to locate other stable contributing conformations, we then performed a 40 ps MD run for **1** with an 8 ps period at 300 K followed by a temperature jump to 600 K for 4 ps, but every 1 ps the simulation was stopped and the remaining structure was energy minimized. Fig. 3 shows four local energy minima and three energy barriers reached by temperature jumps. The first energy minimum of this molecule (1 kcal above the minimum) corresponds to a conformation **AcII**, as in Fig. 2, the cladinose being coplanar with the macrocycle. The second local energy minimum corresponds to a structure of 'higher energy' (3 kcal above the minimum) with a particular conformation of the macrocycle (denoted **B**) in the C(2)–C(3) and C(4)–C(5) region. When the H(3) proton folds inside the erythronolide, then the cladinose sugar moves above the desosamine but its orientation with respect to the macrocycle remains unchanged. This modification does not significantly affect the sugar position (assigned as **b**). The most important deviations (Δ) observed from the X-ray crystal structure (Table 1), are: H(2)–H(3) ($\Delta = -52.5°$); H(4)–H(5) ($\Delta = +26°$); H(5)–Me-6 ($\Delta = +10°$); Ψ1 ($\Delta = -2°$); Ψ2 ($\Delta = +9°$); Ψ3 ($\Delta = +4.5°$); Ψ4 ($\Delta = -10°$). Moreover, a slight deformation (+12°) is observed in the C(13)–O(14)–C(1)–O(1) region (Fig. 4, conformation **Bb**).

The third local energy minimum is the 'higher energy' structure (5 kcal above the minimum) which does not appear in the first protocol. Its macrocycle conformation is like that of the crystal structure (**A**), except for the cladinose orientation, which is turned back (**d** conformation). The deviations from the X-ray structure are: H(2)–H(3) ($\Delta = +8°$); H(4)–H(5) ($\Delta = +11°$); H(5)–Me-6 ($\Delta = -3°$); C(13)–O(14)–C(1)–O(1) ($\Delta = -5.5°$); Ψ1 ($\Delta = -2°$); Ψ2 ($\Delta = +11°$); Ψ3 ($\Delta = -56°$); Ψ4 ($\Delta = -45°$) (Fig. 4, conformation **Ad**).

With protocol II, we have generated two conformations of 'higher energy'—**Ad** with a turned-back cladinose and **Bb** with H(3) folded inside the erythronolide. These conformations are generated while isomerization of the oxime chain occurs [$E \Longleftrightarrow Z$ for the C(8)–C(9)=N(9)–O(16) double bond]. This

Table 3 Qualitative nuclear Overhauser enhancement data for roxithromycin (**1**). Comparison of distances from minimized structures derived from MD at 300 K

	Proton connected			
		MD Structures[a]		
Proton observed	NOE[b]	**AaII**	**BbI**	**AcII**
Inter-unit contacts				
Macrocycle–oxime				
19-OMe	3(m), 6-OH(s), 5″-Me(m), 1″(m)	3*, 2-Me*, 1″, *5″-Me*	6-Me*, *5′-Me*, 5″-Me	*2-Me*; 1″; 2″; 3*
18	3(m), 6-OH(m), 6-Me(s)	3; 6-OH; 6-Me; *5″-Me*, 2-Me*; 5*; 1″	6-Me	3; 6-OH; 6-Me; 2-Me*; 5*; 1″*
17	6-OH(m), 6-Me(m), 11-OH(s)	6-OH*; 11-OH*	*6-OH* 6-Me; *5″-Me*	6-OH*; 6-Me*
16	11-OH(m), 11(s)	11-OH	11-OH	11-OH; 6-OH*; 6-Me*
Macrocycle–sugar rings				
1′	5(l), 4-Me(m)	5; *4-Me*	5; *4-Me*	5; *6-Me*
1″	3(l), 2-Me(m)	3; 2-Me	3; 2-Me	3; 2-Me
2″e	2-Me(s)	2-Me	2-Me	2-Me
3″-OMe	4-Me(m)	4-Me	4-Me	4-Me
5″	5(l)	5	5; *6-Me*	5
5″-Me	6-Me(s), 5(m), 19-OMe(m)	6-Me; 5*; 19-OMe*	6-Me; 5*; 6-OH*; 17; 19-OMe*	5; 6-Me
Desosamine–cladinose				
1′	5″(l), 3″-OMe(m)	*5″*; *3″-OMe*; 4″-OH	*3″-OMe*	*5″*; *5″-Me*
3′	3″-OMe(m)	*3″-OMe*; *4″-OH*		*5″-Me*; 5″*
5′	5″(l), 5″-Me(m)	*5″*; 5″-Me*; *4″-OH*	3″-OMe*; 4″-OH	5″-Me*
3′-N (Me)$_2$	3″-OMe(s)	*3″-OMe**		4″-OH*
Intra-unit contacts				
Macrocycle				
3	2(m), 4(l), 5(l), 6-OH(m), 11(s)	4; 5	*2*; 4; 5; *11*	*2-Me*; 4; 5
4	2(m), 3(l), 6-OH(m), 7a(l), 11(l), 12-Me(m)	2; 3; 5; 7a; *11*; 4-Me	2; 3; 5; 7a; 4-Me	2; 3; 5; 7a; *11*; 4-Me; *12-Me*
6-OH	3(m), 4(m), 5(m), 11(m)	6-Me; 11	6-Me; *8*; 11; *11-OH*	6-Me; *8*; 11
11	4(l), 7(m), 10(s), 13(m), 11-OH(l), 6-OH(m), 12-Me(m)	4; 7; 10; 13; 12-Me; 11-OH; 6-OH	*3*; 4; 7; 10; 13; 12-Me, 11-OH; 6-OH	4; 7; 10; 13; 12-Me, 11-OH; 6-OH
11-OH	11(l), 13(m), 12-Me(s)	10-Me; 11; 12-OH	*6-OH*; 10-Me; 11; 12-OH	10-Me; 11; 12-OH
12-OH	10-Me(m), 12-Me(m), 13(m), 14e(s)	10-Me; 11-OH; 13	10-Me; 11-OH; 13	10-Me; 11-OH; 13
13	11(m), 12-OH(m), 11-OH(m), 15-Me(l), 14e(l)	11; 12-OH; 15-Me; 14e	11; 12-OH; 14e, 15-Me	11; 12-OH; 14e, 15-Me

[a] These values are given by molecular dynamics in three different conformations minimized at 12 and 65 ps (**AaII**, **BbI**) for roxithromycin and at 78 ps (**AcII**) for protonated roxithromycin. The typical spatial proximities of each conformation are italicized (less than 3 Å). Some evident intra-unit contacts found for the different structures are not specified; *interactions between protons more than 3 Å apart. [b] l = large, >5%; m = medium, >1%, <5%; s = small, <1%.

isomerization, while improbable in solution, is due to a weak force constant for the C(8)–C(9)=N(9)–O(16) torsion (0.4 kcal rad^{-2}) calculated by 'automatic assignment parameters.' Thus in the following protocols, this constant has been raised to a value of 12 kcal rad^{-2} on the model of $^{13}C{=}^{13}C$ double bond and no further $E \Longleftrightarrow Z$ isomerization occurred. Fig. 4 shows stereoscopic views of the backbones of these two 'higher minima' **Ad** and **Bd**.

Protocol III (Fig. 5). This protocol was carried out with no raising of the temperature (300 K) but using a long timescale (100 ps) with energy minimization every 1 ps. The initial structure is still the X-ray conformation of the roxithromycin. Molecules generated during this experiment are mainly (95%) of **Aa** type of lowest energies (80% from 66 kcal mol^{-1} to 69 kcal mol^{-1}). This **Aa**-type conformation is in equilibrium with the remaining 5% of **Bb** conformation, which are of higher energy (from 72 kcal mol^{-1} to 73 kcal mol^{-1}). This experiment does not provide a conformation of intermediate energy such as the **Ac** type with a parallel positioning of the desosamine moiety and the macrocycle.

Tables 4 and 5 show the averages and the fluctuations of the dihedral angles. The values reported in Table 6 allow us to characterize the different conformations of the macrocycle, the sugars rings and the oxime chain. Table 6 sums the exploration of conformational space covered during the simulation at 300 K (dihedral angles, spatial proximities, hydrogen bonding and potential energy for each conformation type).

If we analyse the amplitude of the movement of the endocycle torsion angles (Table 4 and Fig. 6) in the macrocycle, the greatest deviation (61°) is observed for the C(2)–C(3) dihedral angle, with smaller effects on the neighbouring C(4)–C(5) (27°) and C(5)–C(6) (16°). This motion, illustrated in Fig. 7, generates the **B** type conformation (5% of the structures), which is also seen in protocol **II** with temperature jumps. In this **Bb** conformation (Fig. 8), a large rotation (46°) of the dihedral angle

Table 4 Evolution of endocycle torsion angles (°) around erythronolide ring in 100 structures minimized each picosecond, for roxithromycin (**1**) and protonated roxithromycin (**2**) (MD at 300 K)

	Amplitude		Average values		Predominant values (%)		0 ps		50 ps		100 ps	
Torsion angles φ	**1**	**2**	**1**	**2**	**1**	**2**	**1**	**2**	**1**	**2**	**1**	**2**
C(1)-C(2)-C(3)-C(4)	61	56	−73	−74	−76 (60)	−75 (62)	−74	−74	−69	−75	−76	−70
C(2)-C(3)-C(4)-C(5)	12	8	164	161	160 (68)	161 (67)	161	161	160	160	160	159
C(3)-C(4)-C(5)-C(6)	27	22	−91	−95	−96 (66)	−95 (54)	−100	−97	−92	−96	−95	−93
C(4)-C(5)-C(6)-C(7)	16	21	−73	−78	−78 (67)	−77 (62)	−76	−78	−78	−78	−78	−78
C(5)-C(6)-C(7)-C(8)	6	5	176	177	177 (64)	178 (76)	177	177	178	178	178	179
C(6)-C(7)-C(8)-C(9)	6	5	−69	−69	−69 (94)	−69 (83)	−71	−69	−68	−69	−69	−67
C(7)-C(8)-C(9)-C(10)	11	12	−68	−67	−66 (63)	−65 (55)	−62	−66	−69	−66	−66	−70
C(8)-C(9)-C(10)-C(11)	16	14	114	112	114 (53)	112 (61)	113	113	102	113	113	101
C(9)-C(10)-C(11)-C(12)	13	12	−164	−167	−168 (62)	−168 (78)	−171	−168	−165	−168	−168	−165
C(10)-C(11)-C(12)-C(13)	13	13	171	172	170 (91)	170 (87)	169	170	180	170	170	180
C(11)-C(12)-C(13)-O(14)	9	10	−65	−69	−69 (89)	−70 (88)	−72	−70	−62	−70	−70	−62
C(12)-C(13)-O(14)-C(1)	40	32	112	109	110 (45)	110 (54)	113	111	99	110	110	99
C(13)-O(14)-C(1)-C(2)	21	21	176	172	173 (94)	172 (84)	174	172	170	172	172	170
O(14)-C(1)-C(2)-C(3)	19	9	117	115	116 (76)	117 (72)	117	116	116	117	117	116

[a] We have reported the amplitude, the average and the main values of endocycle torsion angles for the 100 minimized generated structures, with their statistical participation (in %). They illustrate the final conformations at 100 ps of roxithromycin (**1**) and of protonated roxithromycin (**2**), and their corresponding initial conformations at 0 ps.

Table 5 Evolution of torsion angles (°) in 100 structures minimized each picosecond, for roxithromycin (**1**) and protonated roxithromycin (**2**) (MD at 300 K)[a]

	Amplitude		Average values		Predominant values (%)		0 ps		50 ps		100 ps	
Torsion angles φ	**1**	**2**	**1**	**2**	**1**	**2**	**1**	**2**	**1**	**2**	**1**	**2**
Macrocycle												
H(2)-C(2)-C(3)-H(3)	68	63	161	161	159 (63)	159 (62)	159	161	166	159	159	166
H(3)-C(3)-C(4)-H(4)	10	7	−72	−73	−73 (68)	−73 (75)	−72	−72	−74	−73	−73	−74
H(4)-C(4)-C(5)-H(5)	32	25	139	137	135 (68)	136 (79)	131	133	140	135	136	138
H(5)-C(5)-C(6)-C(6)Me	15	21	46	43	43 (67)	44 (68)	46	44	43	43	43	44
H(7)-C(7)-C(7)-H(8)$_{eq}$	5	4	−69	−69	−69 (75)	−69 (90)	−71	−69	−69	−69	−69	−68
H(7)-C(7)-C(8)-H(8)$_{ax}$	5	4	179	178	179 (74)	179 (90)	177	178	179	178	178	180
H(8)-C(8)-C(9)-C(10)	11	12	171	172	173 (61)	173 (82)	177	177	170	173	173	169
H(10)-C(10)-C(11)-H(11)	10	9	69	67	65 (68)	66 (95)	63	66	67	66	66	66
H(11)-C(11)-C(12)-C(12)Me	15	15	−72	−72	−73 (72)	−74 (86)	−75	−74	−63	−74	−74	−63
C(12)Me-C(12)-C(13)-H(13)	8	10	179	179	179 (90)	179 (82)	176	178	−174	178	178	−174
H(13)-C(13)-O(14)-C(1)	46	36	−9	−9	−8 (45)	−9 (50)	−5	−7.5	−20	−8	−8	−20
H(13)-C(13)-C(14)-H(14)$_{eq}$	5	4	70	69	70 (99)	69 (91)	70	69	70	69	69	70
H(13)-C(13)-C(14)-H(14)$_{ax}$	5	4	−174	−175	174 (99)	−174 (79)	−175	−175	−174	−175	−175	−174
Glycosidic bonds												
H(5)-C(5)-O-C(1′)	9	45	16	3	16 (92)	12 (56)	15.5	15	16	12	16	13
C(5)-O-C(1′)-H(1′)	17	57	40	35	39.5 (93)	43.5 (64)	41.4	40	40	42	40	43
H(3)-C(3)-O-C(1″)	17	19	28	26	28 (90)	27 (62)	29	28	26	28	28	26
C(3)-O-C(1″)-H(1″)	13	16	45	44	46 (60)	46 (62)	48.5	49	46	46	46	47
Oxime chain												
H(17)-C(17)-C(18)-H(18a)	128	123	71	75	63 (82)	63 (75)	−49	62.5	62	63	63	63
H(17)-C(17)-C(18)-H(18b)	127	118	−175	174	179 (82)	179 (79)	68	179	179	180	179	179

[a] We have reported the amplitude, the average and the main values of torsion angles of vicinal proton and some heteronuclear $^{1}H-^{13}C$ dihedral angles of the macrocycle, for the 100 minimized generated structures, with their statistical participation (in %). They illustrate the final conformations at 100 ps of roxithromycin (**1**) and of protonated roxithromycin (**2**), and their corresponding initial conformations at 0 ps.

C(13)–O(14) is observed, which affects the O(14)–C(1) (21°) dihedral angle (Fig. 6 and 7). However we observe a slight rotation of the two glycosidic bonds (17°) for $\Psi 2$ [C(5)–O(5)–C(1′)–H(1′)] and $\Psi 3$ [H(3)–C(3)–O(3)–C(1″)], involving a **b** conformation of the sugar moieties (Fig. 5).

The evolution of the model at 300 K (Fig. 5) shows that after the **Bb** conformation, the model goes through an **Aa** type conformation, but with different energies according to the type of hydrogen bonding. Thus, 9% of the **Aa** conformation is characterized by type **III** hydrogen bonding [11-OH///O=C(1); 6-OH///O(16); 12-OH///OH-11; 4″-OH///OMe-3″] and by the following values of dihedral angles H(2)–H(3) = 166° (Δ = +7); H(4)–H(5) = 140° (Δ = +5); H(11)–Me-12 = −63° (Δ = +11); H(3)–C(1) = −20 (Δ = −12), (the Δ value represents the difference / the predominant values during MD, reported in Table 5). The realization of this type **III** hydrogen bonding is linked to the deformation of the macrocycle in the regions C(9)–C(10)–C(11) and C(13)–O(14)–C(1) (Fig. 7). Furthermore, 22% of the **Aa** structures generated present type **I** hydrogen bonding with higher energy (12% from 72 kcal

Table 6 The different conformational parameters of each unit in 100 minimized structures for roxithromycin (**1**) (MD at 300 K)

	Macrocycle conformation		Hydrogen bonding types[a]			Oxime chain conformation				Sugar conformation	
	A (95%)	**B** (5%)	**I** (27%)	**II** (64%)	**III** (9%)	92%	6%	1%	1%	**a** (95%)	**b** (5%)
Dihedral angle/deg											
H(2)–H(3)	159	117	164	159	166						
H(3)–Me(2)	−82	−125	−78	−82	−76						
M(3)–C(1)	41	2.5	46	41	48						
H(3)–H(4)	−73	−70	−67	−73	−74						
H(4)–H(5)	135	146	135	136	140						
H(5)–Me(6)	43	55	46	43	43						
H(7)–H(8)	−69	−67	−71	−69	−68						
H(8)–C(10)	173	165	168	173	170						
H(10)–H(11)	65	65	71	66	66						
H(11)–Me(12)	−73	−76	−72	−74	−63						
H(13)–C(1)	−8	10	−12	−7.5	−20						
H(17)–H(18a)						62	68	61	−172		
H(17)–H(18b)						−179	−177	177	−57		
H(18a)–C(19)						60	−17	133	163		
H(18b)–C(19)						−59	−135	16	48		
H(5)–C(5)–O–C(1′)[b]										16	16
C(5)–O–C(1′)–H(1′)[b]										39	51
H(3)–C(3)–O–C(1″)[b]										27	35
C(3)–O–C(1″)–H(1″)[b]										46	43
E_p/kcal											
66/68	60%	—	3%	52%	5%	59%	—	1%	—	60%	—
68/70	22%	—	8%	12%	2%	18%	4%	—	—	22%	—
70/72	5%	—	4%	—	1%	5%	—	—	—	5%	—
72/74	8%	5%	12%	—	1%	10%	2%	1%	—	8%	5%

Spatial proximity[c]

H observed	H connected		H connected	
H(2)	15	**3**, 11, 1		
Me(2)	15, 19, 18	**Me(4)**		
H(3)	Me(6), 19, **18**	2, 7a		
H(4)	**5**, 10			
Me(4)	Me(12), 2′			
H(5)	18	10, 1″		
Me(6)		19, 17, 2′, 5″		
HO(6)	**18**	8, 10, **17**, Me(5″)		
H(11)		2, 3		
OH(11)		**OH(6)**		
H(16)				
H(17)				**Me(5″)**
H(18)			**Me(5″)**, 1″	
H(19)			**1″**	**Me(5′)**
H(1′)			5″, OH(4″)	
OH(2′)			OMe(3″)	
H(3′)			**OMe(3″)**, OH(4″)	
NMe_2			OMe(3″)	
H(5′)			5″, Me(5″)	OMe(3″)
Me(5′)			5″	OH(4″)

[a] Hydrogen bonding types: **I**-6OH///O16; 12OH///OH11; 4″OH///OMe3″. **II**-6OH///O17; 12OH///OH11; 4″OH///OMe3″. **III**-11OH///O=C1; 6OH///O16 or (6OH///O16 and 6OH///O17); 12OH///OH11; 4″OH///OMe3″. [b] Glycosidic bonds: Ψ1: H(5)–C(5)–O(5)–C(1′); Ψ2: C(5)–O(5)–C(1′)–H(1′); Ψ3: H(3)–C(3)–O(3)–C(1″); Ψ4: C(3)–O(3)–C(1″)–H(1″). [c] Only the typical spatial proximities of each conformation are presented: 3 Å < inter-proton distances < 4 Å. Close spatial proximities, ≤2.5 Å, are given in bold.

mol^{-1} to 74 kcal mol^{-1}). This type **I** hydrogen bonding is characterized by the association 6-OH///O(16) being less stable and its presence affects the torsion angles C(2)–C(3), C(5)–C(6) and C(13)–O(14) (Fig. 7).

Finally, the conformations **Aa** of type **II** (64%) of lowest energies (from 66 to 69 kcal mol^{-1}) seem to be in good agreement with NMR data as in the previous protocols.

This MD protocol shows that the overall energy minimum structures **AaII** (52%), **AaIII** (5%) and **AaI** (3%) are 2 kcal mol^{-1} dependent (from 66 to 68 kcal mol^{-1}). Roxithromycin is best described as having a single conformation, type **Aa**, with different hydrogen bonding. The conformation **Bb** is unlikely.

Protocol IV (Fig. 9). In order to take account of the polarization state of this molecule and to check for eventual structural effects due to protonation of the dimethylamino group, a molecular dynamics simulation was performed on the protonated roxithromycin **2**. The X-ray crystal structure was

Table 7 The different conformational parameters of each unit in 100 minimized structures for protonated roxithromycin (**2**) (MD at 300 K)

	Macrocycle conformation			Hydrogen bonding types[a]			Oxime chain conformation		Sugar conformation		
	Aa (75%)	**Ac** (24%)	**Bb** (1%)	**I** (5%)	**II** (82%)	**III** (13%)	95%	5%	**a** (75%)	**b** (1%)	**c** (24%)
Dihedral angle/deg											
H(2)–H(3)	159	165	109	166	159	169					
H(3)–H(4)	−73	−74	−69	−71	−73	−74					
H(4)–H(5)	136	139	156	133	135	142					
H(5)–Me(6)	44	40	55	46	43	43					
H(7)–H(8)	−69	−69	−70	−71	−69	−69					
H(10)–H(11)	65	67	64	68	66	67					
H(11)–Me(12)	−74	−74	−76	−73	−74	−63					
H(13)–C(1)	−9	−10	12	−9	−8	−20					
H(13)–Me(12)	178	178	178	179	178	−174					
H(17)–H(18a)							63	−50			
H(17)–H(18b)							−179	66			
H(5)–C(5)–O–C(1′)[b]									12	11	−26
C(5)–O–C(1′)–H(1′)[b]									43	60	8
H(3)–C(3)–O–C(1″)[b]									27	35	20
C(3)–O–C(1″)–H(1″)[b]									46	44	38
E_p/kcal											
90/92	59%	9%	—	2%	64%	2%	68%	—	59%	—	9%
92/94	11%	11%	—	1%	14%	7%	18%	4%	11%	—	11%
94/96	5%	4%	1%	2%	4%	4%	9%	1%	5%	1%	4%
Spatial proximity[c]											
H observed	H connected								H connected		
H(2)	Me(12)	OMe(3″)	**3**, 11, 1″								
Me(2)	15, 19	**3**	**Me(4)**								
H(3)	19, **18**	**Me(12)**	2, 7a								
H(4)		**Me(12)**									
Me(4)	**1′**	2′, 5″	**5**								
H(5)	5′	**OH(2′)**, 1″, **Me(5″)**	Me(5′)								
Me(6)			19, 17, 2′, 5″								
OH(6)			**7a**, 10, **17**, 19, Me(5″)								
H(11)			2, **3**, 17								
OH(11)			**OH(6)**, 18, 19								
H(13)	Me(8)		19								
H(16)										Me(5″)	
H(17)										**Me(5″)**	
H(18)									**Me(5″)**, 1″	1″	
H(19)									**Me(5″)**	**Me(5′)**	2″a
H(1′)									**OMe(3″)**		**Me(5″)**
OH(2′)										NH$^+$	**5″**, OH(4)
H(3′)									**OMe(3″)**	**NH$^+$**	**Me(5″)**, 5
NMe$_2$										NH$^+$	OH(4″)
H(5′)									5″	OMe(3″)	Me(5″)
Me(5′)									5″	OH(4″)	

[a] Hydrogen bonding types: **I**-6OH///O16; 12OH///OH11; 4″OH///OMe3″; NH$^+$///OH2′; OH2′///O5. **II**-6OH///O17; 12OH///OH11; 4″OH///OMe3″; NH$^+$///OH2′; OH2′///O5. **III**-11OH///O=C1; 6OH///O16 or (6OH///O16 and 6OH///O17); 12OH///OH11; 4″OH///OMe3″; NH$^+$///OH2′; OH2′///O5. [b] Glycosidic bonds: Ψ1: H(5)–C(5)–O(5)–C(1′); Ψ2: C(5)–O(5)–C(1′)–H(1′); Ψ3: H(3)–C(3)–O(3)–C(1′); Ψ4: C(3)–O(3)–C(1″)–H(1″). [c] Only the typical spatial proximities of each conformation are presented: 3 Å < inter-proton distances < 4 Å. Close spatial proximities, ≤2.5 Å, are given in bold.

modified for a protonated molecule and the charges recalculated[18] using the DISCOVER algorithm (Dinur–Hagler), with a total charge of +1.

The structure was previously energy minimized (96 kcal mol^{-1}, 5 kcal above the minimum) and we performed 100 ps of MD at 300 K (as described in protocol III). In Tables 4 and 5 the amplitudes of endocycle torsion angles for the protonated roxithromycin are reported (in italics) and a weak attenuation compared with the unprotonated molecule can be noticed, approximately −5° in the C(1) to C(5) region, and also a reduction of 8 or 10° in the C(12)–C(1) [or H(13)–C(1)] region. In contrast, a slight increase of +5° for the C(5)–C(6) torsion angle is also noticed. This is sufficient to significantly affect the mobility around the glycosidic bonds, +36° and +40° for Ψ1 and Ψ2, respectively. This induces conformation **c** which represents 24% of generated structures in this experiment (Table 7). The most important variations of the dihedral angles are reported in Tables 4, 5 and 7. In the case of the protonated molecule, we find the same high amplitudes for the endocyclic torsion angles such as C(2)–C(3) (56°), C(4)–C(5) (22°) and C(5)–C(6) (21°). This will induce the different conformations **A**, and **B** of the macrocycle in these regions and a significant mobility of the two sugars (conformations **a**, **b**, **c**). All the dihedral angles from C(8) to C(12) have a mean amplitude of

Table 8 Notation for conformer designations defined as **A**, **B**, **a**, **b**, **c**, **d**, **I**, **II** and **III**

Sugar conformations[a]

Torsion angles/°	**a**	**b**	**c**	**d**
Ψ1	15	10	−25	15
Ψ2	40	60	10	55
Ψ3	25	35	20	−22
Ψ4	45	45	40	−3

Macrocycle conformations[b]

Torsion angles/°	**A(II)**	**B(I)**	**A(III)**
H(2)–H(3)	160	115	165
H(3)–C(1)	40	3	48
H(4)–H(5)	135	145	140
H(5)–Me(6)	43	55	43
H(11)–Me(12)	−73	−76	−63
H(13)–C(1)	−8	10	−20

Hydrogen-bonding types

Type I	Type II	Type III
6-OH///O-16 12-OH///OH-11 or 6-OH///O-16; 11-OH///O-17 12-OH///OH-11	6-OH///O-17 12-OH///OH-11 or 6-OH///O-16; 6-OH///O-17 12-OH///OH-11	11-OH///O=C1; 6-OH///O-16 12-OH///OH-11
Type I*		
11-OH///O-16; 11-OH///O-17 12-OH///OH-11		

[a] The glycosidic dihedral angles: Ψ1, H(5)–C(5)–O(5)–C(1′); Ψ2, C(5)–O(5)–C(1′)–H(1′); Ψ3, H(3)–C(3)–O(3)–C(1″); Ψ4, C(3)–O(3)–C(1″)–H(1″). **a** conformation in which the desosamine orientation is nearly perpendicular to the macrocycle. **b** conformation: H(3) folds inside the macrocycle causing a reorientation of the cladinose above the macrocycle and the desosamine rotates slightly with respect to the macrocycle. **c** conformation in which the desosamine sugar is coplanar with the macrocycle. **d** conformation: the cladinose orientation is turned back. [b] Conformation models **A** and **B** for the aglycones of the 14-membered macrolides. The C(3) to C(5) 'folded-out' type (conformation **A**) and the corresponding C(3) to C(5) 'folded-in' type (conformation **B** or **B′**). Conformation **AIII**: the lactone group C(1)=O, folds inside the macrocycle and allows 11-OH to form a hydrogen bond with C(1)=O.

12°. The modifications in this region are due to the different orientations of the oxime chain and of the 11-OH group, which is able to form hydrogen bonds with C(1)=O (type **III**) or with the different heteroatoms of the oxime chain. Finally, a large amplitude is observed for the C(13)–O(14) and O(14)–C(1) torsions. The region from C(13) to C(2) is rearranged according to the orientations of the C(1)=O group and of the extremity of the oxime chain (often linked to movement of the sugars).

Analysis of the 100 minimized structures generated has shown three different conformations for the sugars, **a**, **b**, **c**, two macrocycle conformations, **A** and **B**, and finally, three types of hydrogen bonding, **I**, **II** and **III** (Figs. 9 and 10). The three different positions of sugar moieties **a**, **b**, **c** appear in Fig. 11 and their characteristics are reported in Table 7. The **a** conformation (75% of generated structures) characterized by a desosamine orientation nearly perpendicular to the macrocycle ($\Psi1 = 12°$, $\Psi2 = 43°$, $\Psi3 = 27°$ and $\Psi4 = 46°$) is differentiated in **AaI**, **AaII** and **AaIII** conformations according to the types of hydrogen bond. The **c** conformation (24% of the generated structures) ($\Psi1 = -26°$, $\Psi2 = 8°$, $\Psi3 = 20°$ and $\Psi4 = 38°$) corresponding to **AcI**, **AcII** and **AcIII**, is characterized by a desosamine sugar coplanar with the macrocycle. Thus, a combination of potential-energy minimum structures, 59% of conformations **AaI**, **AaII** and **AaIII**, and 9% of conformations **AcI**, **AcII** and **AcIII**, 2 kcal above the minimum (from 90 to 92 kcal mol^{-1}), appear to contribute to produce a stable solution conformation.

The **b** conformation ($\Psi1 = 11°$, $\Psi2 = 60°$, $\Psi3 = 35°$ and $\Psi4 = 44°$), with an energy 6 kcal above the minimum, is taken into account only with difficulty in a conformational averaging. This conformation **BbI**, corresponding to 1% of the generated structures, was miminized at '90 ps'. During the simulation, two new hydrogen bonds appear in 100% of the generated structures, 3′-$N(Me)_2H^+$///OH-2′ and 2′-OH///O(5), in addition to the different types of hydrogen bond already existing (**I**, **II**, **III**). Hydrogen bond types are characterized as follows: Type **I** by 6-OH///O(16); Type **II** by 6-OH///O(17); Type **III** by 11-OH///O=C(1), and it is noted that they induce particular deformations of the macrocycle (Fig. 10 and Table 7).

The main conformations of the erythronolide for **2** are either a modified **A** conformation corresponding to the isomers **AaII** or **AcII**, or a conformation **A** deformed in the C(8)–O(14) region, such as the **AaIII** and **AcIII** structures.

Crystal Structure of Roxithromycin.—The X-ray crystal structures of various macrolide antibiotics have been studied[9,19] with the aim of obtaining structure–activity relationships. The crystal structure of erythromycin A is characterized predominantly by a 'folded-out' conformation **A**, whereas two 'folded-in' models **B** and **B′** are found with the crystal structure of two derivatives of erythromycin A (Table 1). The 'folded-out' conformation **A** is characterized by the close cross-ring approach of H(4) and H(11) (NOE[11]^4). In the 'folded-in' conformation (**B** or **B′**), rotation, principally about C(2)–C(3) and C(5)–C(6), causes the C(3)–C(5) portion of the macrocyclic ring to 'fold inwards' such that H(3) gets closer to H(11) (NOE[11]3). However, the similarity in the $\varphi_{C(3)C(4)}$ and $\varphi_{C(4)C(5)}$ angles of the crystal structures of erythromycin A (conformation **A**) and its derivatives (conformations **B** and **B′**), implies that the orientation of the sugar rings (conformation **a**) with respect to one another is almost the same for both substances.

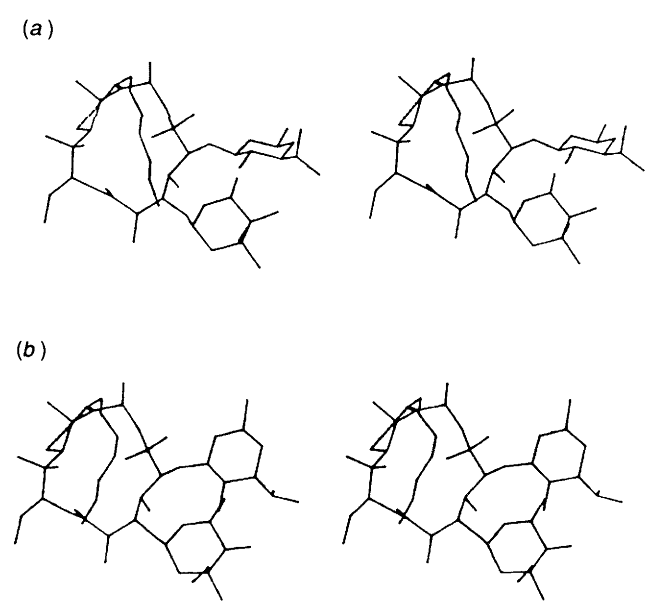

Fig. 2 *Protocol I.* Stereoscopic view of roxithromycin conformations. (*a*) **AaII**. From NMR data, the oxime chain is anchored to the erythronolide by the 6-OH group and the close approach of 19-OMe and H(3), as observed by NOE (Table 3), is then confirmed. Thus the cladinose sugar bonded in C(3) pushes back on the desosamine, which consequently loses some of its mobility, and the two α faces of the cladinose and the desosamine rings face each other. (*b*) **AcII**. The oxygen atom O(17) of the oxime chain is engaged in hydrogen bonding with 6-OH of the macrocycle, and the chain is orientated above the macrocyclic lactone ring with 19-OMe and the carbonyl group, C(1) = O in close proximity. Thus the cladinose sugar recovers some of its mobility and consequently the motions of desosamine and cladinose sugar lead to this coplanar orientation **c**.

It was therefore of interest to investigate the different conformations of the aglycone and the sugar rings in roxithromycin (**1**) and protonated roxithromycin (**2**). Table 1 compares the lactone ring torsion angles for the crystal structures of roxithromycin[15] (type **A**) and of erythromycylamine derivatives[10] (type **B** or **B′**) with conformations generated by molecular dynamics data, conformations miminized at 12 and 65 ps (**BbI**, **AaII**) for roxithromycin and at 67, 78 and 90 ps (**AaII**, **AcII**, **BbI**) for protonated roxithromycin. In Table 1, only a slight rotation about C(5)–C(6) is observed for the structures minimized at 12 ps and 90 ps from data from **1** and **2** respectively. For these two structures, the torsion angles are similar in the C(1)–C(2), C(2)–C(3), C(13)–O(14) and O(14)–C(1) portions of the aglycone conformation **B′** (or **B**) but they differ from **B′** mainly in the C(5)–C(6) and C(7)–C(8) regions. Thus by analogy, in the analysis of minimized structures derived from MD, the macrocycle conformations fall into two distinct groups, type **A** and type **B**. In these conformers the relative orientations of the sugar rings depend on the rotation principally about the C(4)–C(5) and C(5)–C(6) bonds. The structures observed by MD confirmed the tendency of the desosamine sugar to adopt a conformation **a** with an orientation nearly perpendicular to the macrocyclic lactone ring whereas the two units appear to be in the same plane, with conformation **c** for 24% of structures from **2**.

Complete analysis of structures generated by MD shows that compounds **1** and **2** exist as a conformational blend with exchange between conformational types (Fig. 13). There is a division into two groups **Aa** and **Bb** for **1** and into three groups **Aa**, **Ac** and **Bb** for **2**. For **1**, those designated as type **A** are all found to populate preferentially a conformation modelled on **Aa** and for **2**, two conformations modelled on **Aa** and **Ac**. Type **B** members preferentially populate a conformation modelled on **Bb**.

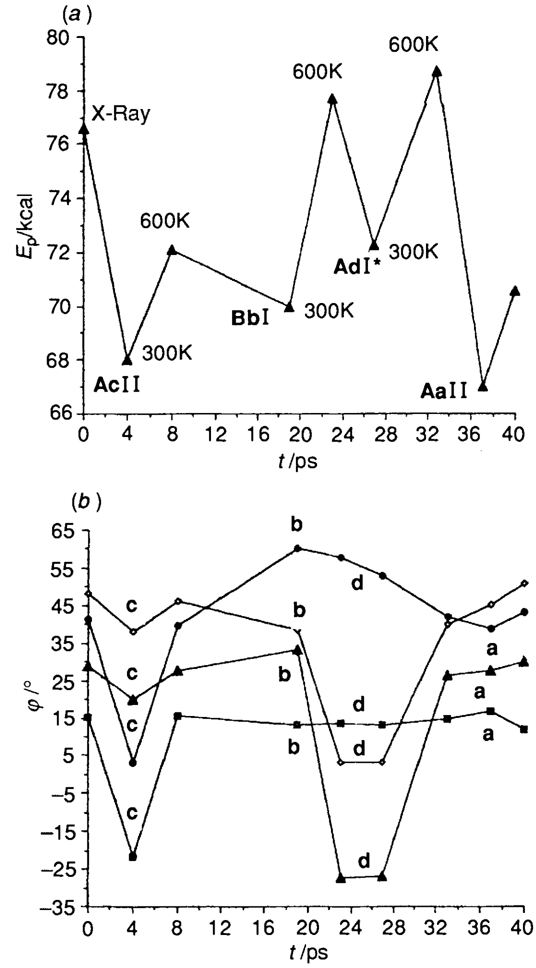

Fig. 3 *Protocol II.* (*a*) Variation of potential energy *vs.* time for minimized structures for roxithromycin. (*b*) Variation of glycosidic angles Ψ1 [■, H(5)C(5)OC(1′)], Ψ2 [●, C(5)OC(1′)H(1′)], Ψ3 [▲, H(3)C(3)OC(1″)] and Ψ4 [○, C(3)OC(1″)H(1″)].

In Table 1 the torsion angles around the macrocycle are compared for type **A** conformers, **Aa** and **Ac** and type **B** conformers, **Bb**. Their three-dimensional structures are quite similar. The torsion angles are similar for the C(6)–C(13) portion of the aglycones, but they are different for the C(1)–C(3), C(4)–C(6) and C(13)–O(14) regions of the molecule. Rotation about the C(2)–C(3), C(4)–C(5) and C(5)–C(6) bonds leads to an increase of *ca.* 6° (**Aa**), 2° (**Ac**), 50 (**Bb**) in $\varphi_{C(2)C(3)}$, to a decrease of *ca.* 9° (**Aa**), 13° (**Ac**), 25° (**Bb**) in $\varphi_{C(4)C(5)}$ and to an increase of *ca.* 5° (**Aa**), 9° (**Ac**), or a decrease of *ca.* 7° (**Bb**) in $\varphi_{C(5)C(6)}$, in comparison with the crystal structure of **1**. These data suggest that conformational instability exists in the C(3)–C(6) region of the native substance. Furthermore, reorganization of another portion of the ring [C(13)–O(14)–C(1)–C(2)] has caused $\varphi_{C(13)O(14)}$, $\varphi_{O(14)C(1)}$ and $\varphi_{C(1)C(2)}$ to evolve differently. This indicates that the orientation of the sugar rings with respect to one another and with respect to the lactone ring in **1** and **2** and, at the same time, the orientation of the lactone group, are slightly different to that found in the solid state and are different for both conformations.

Thus from ^{1}H NOE experiments, ^3J ^{1}H–^{1}H and ^3J ^{13}C–^{1}H coupling constant data in solution provide excellent monitors of the macrocyclic lactone ring folding about C(3) or of the rotation about C(2)–C(3) and C(4)–C(5) bonds and of the relative orientation of the sugar rings.

Conformational Analysis in Solution.—The conformational analysis of the macrolide is difficult in this case, because a

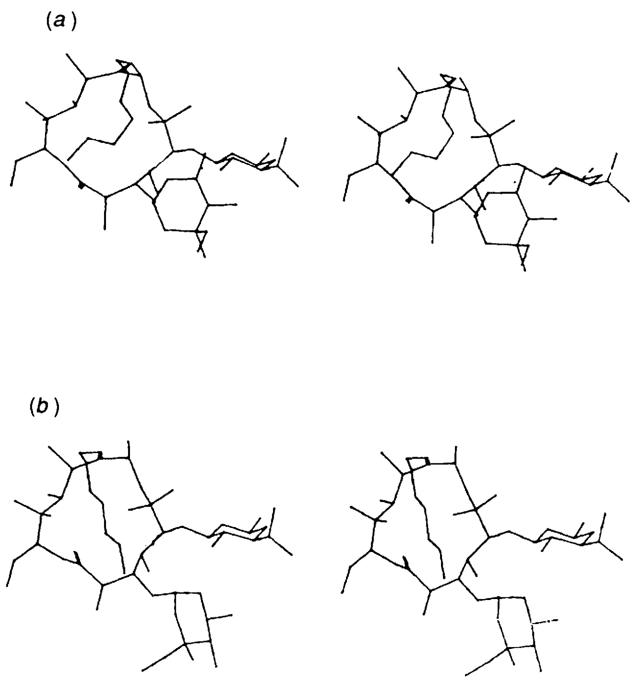

Fig. 4 *Protocol II.* Stereoscopic view of roxithromycin conformations. (*a*) **Bb**. When the H(3) proton folds inside the erythronolide, the cladinose sugar goes above the desosamine but its orientation with respect to the macrocycle remains unchanged. The oxime chain ending on the O(14) level is strongly bound by a hydrogen bond with 11-OH. (*b*) **Ad** The macrocycle conformation is like that of the X-ray structure (**A**), except for the cladinose orientation which is turned back (**d** conformation). The end of the oxime chain above H(3) induces this new orientation of the cladinose moiety.

similar conformation in solution and hence close similarities in the corresponding NMR spectra would be expected, since the two conformers differ only in the flexibility of the three units (macrocycle, oxime chain and particularly desosamine sugar). NMR spectroscopy provides the most reliable information about the structure in solution. The lactone ring in roxithromycin is found to be relatively rigid in solution as there are restrictions on unit mobility in this molecule. Thus it would be expected that much stereochemical and conformational data could be deduced from ^1H–^1H and ^{13}C–^1H coupling constant data.

Determination of ^3J ^1H–^1H *and heteronuclear* ^{13}C–^1H *coupling constants.* We have used the Karplus equation to determine[8,20,21] whether the conformation about the bond is fixed (a single value of φ) or flexible (so that the observed coupling constant is an average of values, corresponding to two or more distinct values of φ). The calculated $^3J_{HH}$ values for the solid-state conformation may be estimated by a Karplus equation such as eqn. (1)[8,21] with $n = 0.1$ and $n = 0.2$, respectively, for

$$^3J = (7.8 - \cos\varphi + 5.6\cos 2\varphi)(1 - n\Sigma\Delta Ex_i) \quad (1)$$

a *trans* and a *cis* coupling constant (an adjustment parameter for the stereochemistry of two vicinal protons), and $\Sigma\Delta Ex_i$ is the electronegativity parameter.

Coupling constants (^3J C–H) across the glycosidic bond were calculated using a newly proposed Karplus-type equation for the C–O–C–H segment [eqn. (2)].[20]

$$^3J_{CH} = 5.7\cos^2\varphi - 0.6\cos\varphi + 0.5 \quad (2)$$

An analysis of ^3J values (Table 2) was used to establish the similarity between the major solution-state conformation of roxithromycin, the X-ray crystal structure and the conforma-

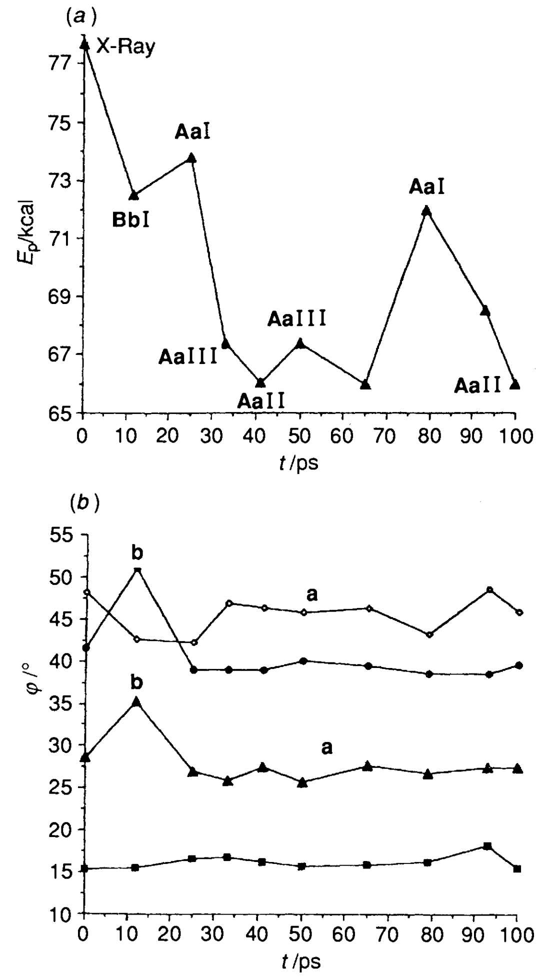

Fig. 5 *Protocol III.* (*a*) Variation of potential energy *vs.* time for minimized structures (at 300 K) for roxithromycin. (*b*) Variation of glycosidic angles Ψ1 [■, H(5)C(5)OC(1′)], Ψ2 [●, C(5)OC(1′)H(1′)], Ψ3 [▲, H(3)C(3)OC(1″)] and Ψ4 [○, C(3)OC(1′)H(1″)].

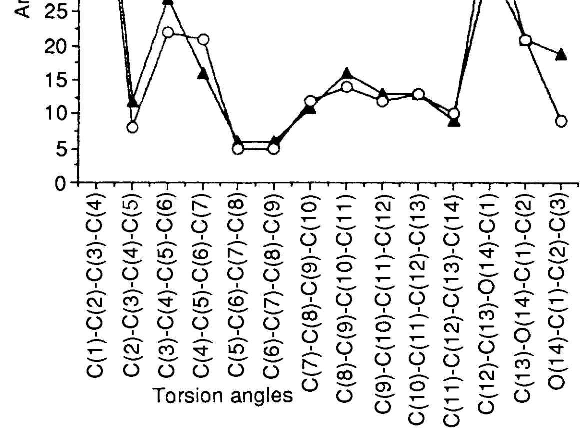

Fig. 6 Amplitude of endocycle torsion angles for roxithromycin (▲) and protonated roxithromycin (○) (MD at 300 K)

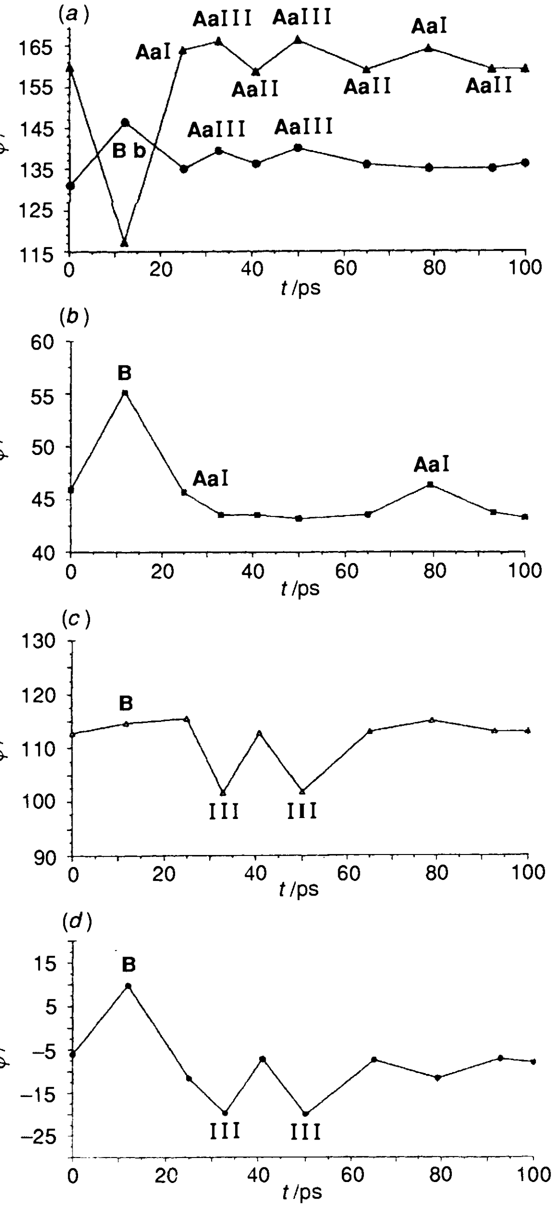

Fig. 7 Variation of dihedral angles around the erythronolide ring for roxithromycin (MD at 300 K): (*a*) ▲ H(2)C(2)C(3)H(3); ● H(4)C(4)-C(5)H(5); (*b*) ■ H(5)C(5)C(6)Me(6); (*c*) △ C(8)C(9)C(10)C(11); (*d*) ● H(13)C(13)O(14)C(1)

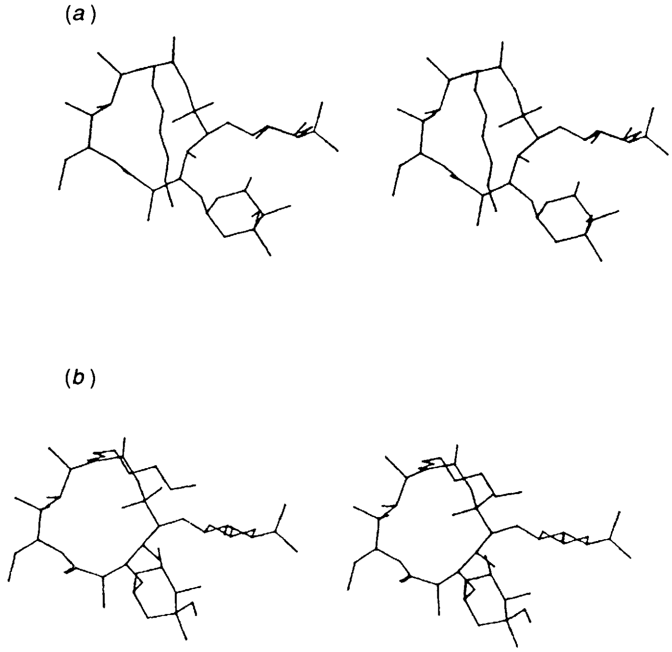

Fig. 8 *Protocol III.* Stereoscopic views of roxithromycin conformations. (*a*) **AaII** minimized at 65 ps. In the **AaII** structure, the end of the oxime chain is situated above the H(3) and H(1″), close to the cladinose sugar. This in turn is pushed back onto the desosamine, which consequently loses some of its mobility and the two α faces of the cladinose and the desosamine rings face each other. (*b*) **BbI** minimized at 12 ps. When H(3) folds inside the macrocycle, it causes a reorientation of the cladinose (Ψ3) above the macrocycle, which allows the desosamine to rotate slightly with respect to the macrocycle. This particular position of the cladinose sugar repels the oxime chain which then moves beyond the desosamine. The 6-OH group is engaged in a type **I** hydrogen bond with O(16). H(17) and H(18) are close to 6-Me and the end of the oxime chain is placed beyond the desosamine with a characteristic spatial proximity between 19-OMe and 5′-Me of <3 Å.

tions generated by MD from **1** and **2**. We observe that the crystal structure conformation cannot account for all of the NMR data. Furthermore, the results of Table 2 show that the other minor conformation(s) participate to a small extent in solution. The observed $^3J_{HH}$ values for the C(2)–C(3) and particularly the C(4)–C(5) regions are slightly different in solution from those calculated for a crystal structure. The small differences between these values are attributed to a slight variation in the dihedral angles. For example, the difference in $J_{4,5}$ with respect to the previously calculated values for the conformer in the solid state is more important. It can be accounted for either by a deformation in the torsion angle C(4)–C(5) for the conformation in solution (a change in orientation of these substituents could increase φ by *ca.* 7°. The predominant form with $\varphi = 137°$ is in better agreement with the experimental data), or by a participation of different coupling constants for the protons H(4), H(5) (from the crystal structure and from **Aa**, **Ac** or **Bb**, respectively). This would result from the presence in solution of other minor conformation(s) that affect conformer **A** (in the solid state) in this region, as is in the case of the 'folded-in' conformation **B**. However, the use of MD simulation allows us to conclude that compound **1** may exist in solution as one major conformer **Aa** and compound **2** as an average of the conformers **Aa** and **Ac**.

Determination of heteronuclear ^{13}C–^1H coupling constants is a useful experiment in the conformational analysis of the molecular region in which homonuclear $^3J_{HH}$ values cannot be measured. This is especially helpful for glycosidic bonds in order to determine the relative positions of the sugar moieties with respect to the erythronolide. Further information may be gained about isolated carbons of the macrocycle such as C(1) [$J_{C(1)H(3)}$ or $J_{C(1)H(13)}$].

Several techniques for this kind of study are available.[22–24] Selective 2D INEPT has the advantage of being easier to analyse because all the homonuclear J_{HH} coupling constants can be suppressed, which is not the case for the reverse experiment.[24b] The ^{13}C signals detected using this appear as discrete doublets (owing to the selective excitation of the corresponding proton). The $^3J_{CH}$ values can be estimated by the sequence shown below.

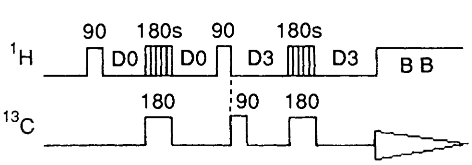

A preliminary adjustment of D3 and the increment delays is necessary in order to avoid too great a loss of ^{13}C signal due to

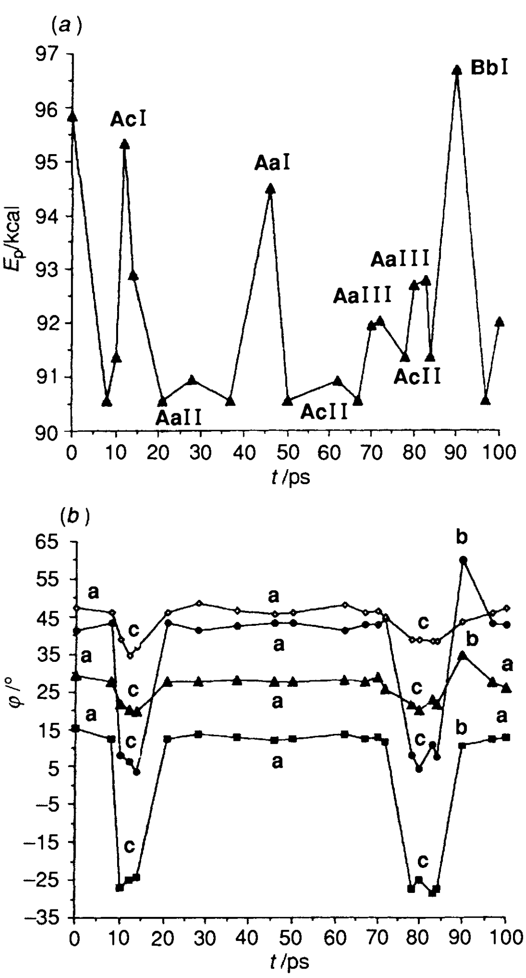

Fig. 9 *Protocol IV.* (*a*) Variation of potential energy *vs.* time for miminized structures (at 300 K) for protonated roxithromycin (**2**). (*b*) Variation of glycosidic angles $\Psi1$ [■, H(5)C(5)OC(1′)], $\Psi2$ [●, C(5)OC(1′)H(1′)], $\Psi3$ [▲, H(3)C(3)OC(1″)] and $\Psi4$ [◇, C(3)OC(1′)H(1″)].

relaxation. This experiment, tested with an α-methyl glucoside (where the J_{CH} coupling constants had been determined by a selective *J* resolved experiment[24d]), showed that J_{CH} coupling constants higher than 2 Hz could be measured with this 2D selective experiment. Usually, in this sequence, the decoupler power is altered four times because of alternation of non-selective and selective pulses, which can be a demanding task for the hardware. In this case, the decoupler power remained the same until the end of the D3 delay and the selective Dante 180° proton pulse[24c] was adjusted subsequently. The power was changed only before broad-band decoupling.

Study of glycosidic bonds began with the selective irradiation of the macrocycle protons H(3) [for $\Psi3$, H(3)C(3)O(3)C(1″) and H(5) [for $\Psi1$, H(5)C(5)O(5)C(1′)] and selective irradiation of the sugar protons H(1′) [for $\Psi2$, C(5)O(5)C(1′)H(1′)] and H(1″) [for $\Psi4$, C(3)O(3)C(1″)H(1″)]. The macrocycle carbon C(1) was studied *via* the H(13) [H(13)C(13)O(14)C(1)] and H(3) protons [H(3)C(3)C(2)C(1)]. All the $^3J_{CH}$ values evaluated are presented in Table 2.

The first step in the analysis of the 2D matrix was to determine the relative intensities of detected signals. J_{CH} coupling constants were measured only for intense doublets with easily readable values. Signals of low intensity may have been due to relaxation or to a low value for the coupling constant and thus weak polarization transfer. Loss of signal by relaxation could be excluded under our experimental conditions as the relaxation parameters are of nearly the same order ($T_2 \approx T_1$) in this molecule. Therefore, when no signal is observed, qualitative information can be extracted, as we know that the J_{CH} constant must be ≤ 2 Hz.

$^3J_{CH}$ Data are correlated with the glycosidic torsion angle found in the different energy-minima models generated by MD. The data do not support a single conformation model for the sugar rings and only conformational averaging gives good agreement between theoretical and experimental data.

Our observed values for $^3J_{C(1')H(5)}$ ($\Psi1$) and $^3J_{C(5)H(1')}$ ($\Psi2$) of 5.3 and 4.5 Hz can be correlated with torsion angles of approximately 14 and 28° respectively, by using eqn. (2). These angles correspond to a shape between **Aa** (16 and 39°) and **Ac** (−27 and 8°). The very small coupling constant measured for $\Psi4$, $^3J_{C(3)H(1'')}$, corresponds to a torsion angle near 50°, which is also compatible with an average conformation between **a** (46°) and **c** (39°). The 1 Hz discrepancy for the coupling constant $^3J_{C(1'')H(3)}$ is not particularly significant and is no larger than the experimental error. It may be interpreted as only a slight variation of the dihedral angle $\Psi3$ (14°), compared with those of **a** (27°) and **c** (22°).

The values of $^3J_{CH}$ measured for the macrocycle $^3J_{C(1)H(3)}$, $^3J_{C(3)H(5)}$, $^3J_{C(6\text{-}Me)H(5)}$, $^3J_{C(11)H(13)}$ and $^3J_{C(15\text{-}Me)H(13)}$ (41, 23, 49, 50, −50 Hz) are similar to those reported for **Aa** (41, 19, 43, 51, −52 Hz) and **Ac** (46, 22, 46, 53, −52 Hz), but differ from the crystal-structure values or the values predicted for the **Bb** conformation. Again the NMR results reflect a possible conformational averaging over the low-energy conformers **Aa** and **Ac** for **2**. Overall, the **AaII** values correspond reasonably well with the experimental results for **1**.

The 2 Hz discrepancy for $^3J_{C(1)H(13)}$ (with respect to the crystal structure or **Aa**, **Ac Bb**) is not particularly significant since this coupling constant changes rapidly with small angular changes in this region. However, the main difference could be due to the effect of an electronegativity parameter sensitive to the orientation of the polar lactone group, such as the carbonyl bond, H(13)–C(13)–O(14)–C(1)=O. We could improve evaluation of this parameter, g ($\Psi_{O=C}$, $\Sigma\Delta Ex'$), a function of the value of the torsion angle $\Psi_{O=C}$ and of the substituent electronegativity, $\Sigma\Delta Ex'$, with the Karplus-type eqn. (3) modified from the predominant form **Aa** with the values of $\varphi \approx \pm 8°$ and $g(\Psi_{O=C}, \Sigma\Delta Ex') = 3.5/5.5 = 0.64$. Such variations with bond orientation have already been observed and discussed[25] for heteronuclear $^3J_{CH}$ values, for the molecular fragment X-^{13}C–CH$_2$–CH$_2$–^{1}H.

$$^3J_{CH} = f(\varphi) * g(\Psi_{O=C}, \Sigma\Delta Ex') \qquad (3)$$

Nuclear Overhauser enhancement (*NOE*) *experiments.* 2D phase-sensitive ^{1}H NOESY experiments in CDCl$_3$ were performed using a time-proportional phase-increment method[26] and different mixing times (τ_m = 200 and 300 ms). Extensive 250 MHz ^{1}H NOE difference experiments in CDCl$_3$ were used to confirm the 2D results. Inspection of the matrix of ^{1}H NOEs for roxithromycin (Table 3) shows whether the pattern of NOEs involving the lactone protons, the oxime chain and interactions involving the sugar units is similar to that found in minimized structures generated by MD (Tables 6 and 7). The observed inter-residue NOE values are compared in Table 3 with spatial proximity values computed from the low-energy conformers having sugars in **a**, **b** and **c** positions (Tables 6 and 7). Table 3 also includes some interesting intra-residue NOEs. The range for the NOE shows how sensitive they can be to the glycosidic linkage conformation (Tables 6 and 7). In contrast, the intra-residue (macrocycle) NOE is almost constant. Differences with other macrolides were observed for some NOEs, particularly those from the methyl groups such as [2-Me]2″eq (**Aa**, **Bb**, **Ac**), [12-Me]4 (**Aa** only), [6-Me]5″Me and protons [4]7ax (**Aa**, **Bb**, **Ac**). The very small NOE [11]3 (**Bb**) is only observed in

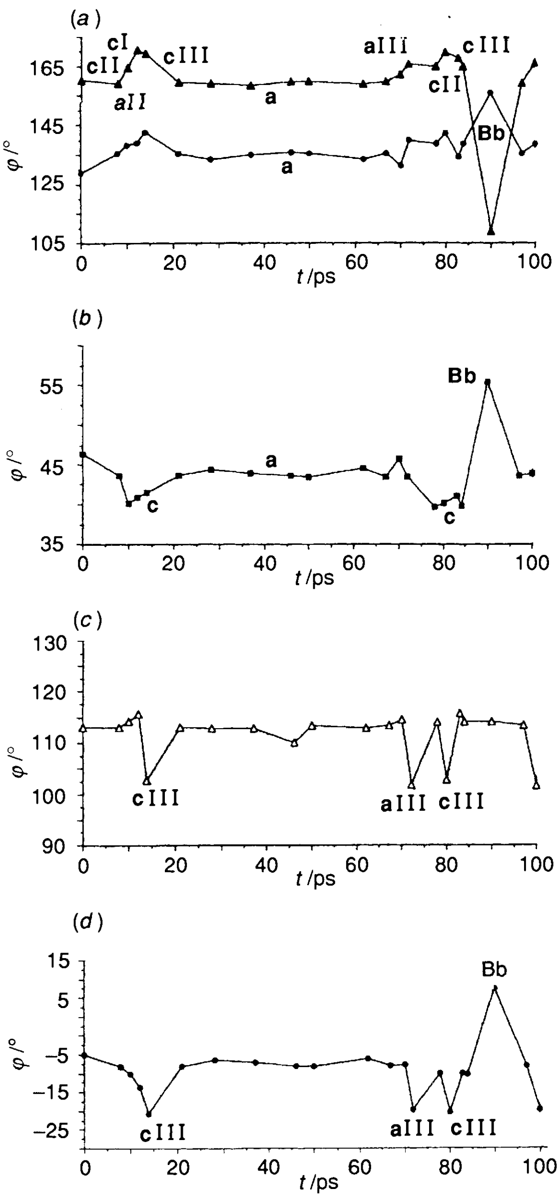

Fig. 10 Variation of dihedral angles around the erythronolide ring for protonated roxithromycin (MD at 300 K); (*a*) ▲ H(2)C(2)C(3)N(3); ● H(4)C(4)C(5)H(5); (*b*) ■ H(5)C(5)C(6)Me(6); (*c*) △ C(8)C(9)C(10)-C(11); (*d*) ● H(13)C(13)O(14)C(1)

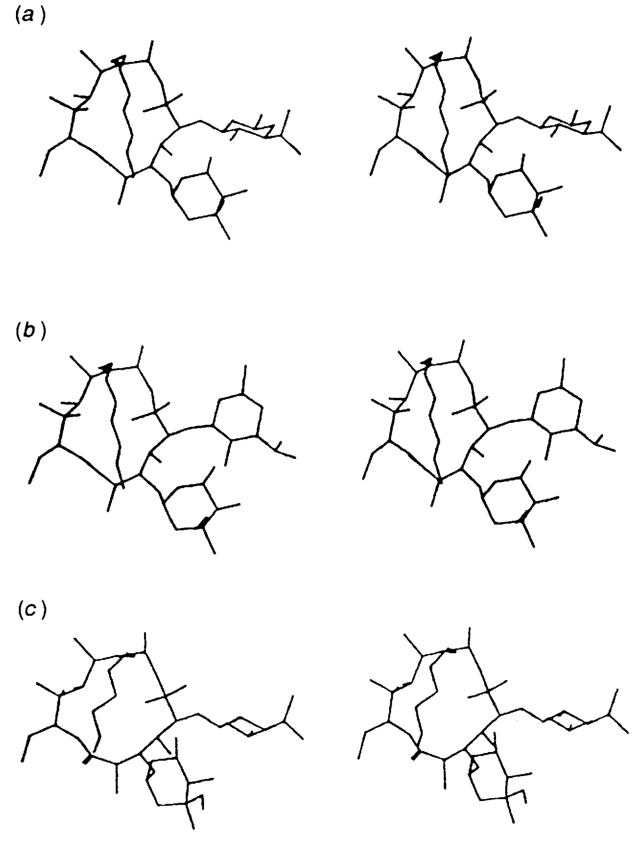

Fig. 11 *Protocol IV.* Stereoscopic views of protonated roxithromycin conformations. (*a*) **AaII** minimized at 67 ps. The end of the oxime chain is situated above H(3) and H(1″), close to the cladinose sugar, which is then pushed back onto the desosamine and the two α faces of the cladinose and the desosamine rings face each other. (*b*) **AcII** minimized at 78 ps. The chain is oriented above the macrocyclic lactone ring with 19-OMe and the carbonyl group C(1)=O in close proximity, and consequently the motions of desosamine and cladinose sugar lead to this coplanar orientation **c**. (*c*) **BbI** minimized at 90 ps. Here H(3) folds into the macrocycle and the cladinose moves above the erythronolide. The oxime chain is then pushed towards the carbonyl C(1)=O, whereas the chain was situated beyond the desosamine for the equivalent structure found in protocol **III** (Fig. 8). This particular position is thus characterized by 19-Me and H(13) being in close spatial proximity.

CD_3OD. Everett and Tyler have already concluded, for erythromycin A, that these unexpected NOEs (NOE[3]11 and NOE[11]3) could be due to a minor conformer **B** in equilibrium with a major one.[9]

For **1**, the phase-sensitive 2D ^1H NOESY in $CDCl_3$ at 300 ms (Table 3) demonstrated the spatial proximity of: 11-OH to H(16); 6-OH and 6-Me to H(17) (**Aa**, **Bb**, **Ac**) and H(18) (**Aa**, **Ac**); H(3) (**Aa**, **Ac**) and 6-OH to 19-Me. We deduced that the oxime chain is directed between C(8) and 11-OH, towards 6-Me and 6-OH and finally that 19-OMe and H(3) are spatially close. The far NOE (only at τ_m = 300 ms) observed at 5″-Me from 19-OMe (**Aa**) shows the presence of the oxime chain close to the cladinose. Three cladinose–lactone NOEs were observed, corresponding to an interaction between the two units: the NOEs [2″eq]2-Me, [1″]2-Me and the NOE [5″-Me]6-Me (**Aa**, **Bb**, **Ac**), which was indicative of the small distance between these two methyl groups. Three inter-sugar NOEs were observed for **1**, the NOEs from 3″-OMe to H(3′) and to 3′-N(Me)$_2$ and the NOE [5″]5′. These inter-sugar NOEs confirmed that the two α faces for the cladinose and the desosamine rings are opposite to each other in **1**, and they are also indicative of inter-sugar interactions characteristic of **Aa** only.

^{13}C NMR relaxation measurements (T_1 data) led to the same conclusions as the NOE data, with respect to the conformation in solution. The presence of the oxime moiety in roxithromycin reduces the mobility of the macrocyclic lactone ring, and consequently the motion of the desosamine and cladinose sugars. T_1 values were used to probe the mobility of the protonated carbons in roxithromycin. These results showed that the desosamine sugar was more mobile than the cladinose sugar and that the lactone ring was more sterically hindered than the other units.[14] Table 5 displays for **2** analogous differences in the amplitudes of torsion angles of the desosamine moiety during a 100 ps simulation, Ψ1 (45°), Ψ2 (57°), with respect to the cladinose ones, Ψ3 (19°) and Ψ4 (16°). The small T_1 values for 6-Me, 8-Me, 10-Me, 12-Me and 15-Me (1.02–1.2 s) were indicative of sterically hindered rotation. They are in good agreement with the amplitude (*ca.* 10°) of torsion angles in the C(6)–C(13) region observed during the MD (Tables 4 and 5, Fig. 6). As for the macrocycle, the ^{13}C NT_1 values for the flexible side chain were small. This result was indicative of the contribution of the oxime chain conformation that restricted its rotation and is in agreement with the existence of a hydrogen bond between the oxygen atom of the oxime chain and the

(*a*)

(*b*)

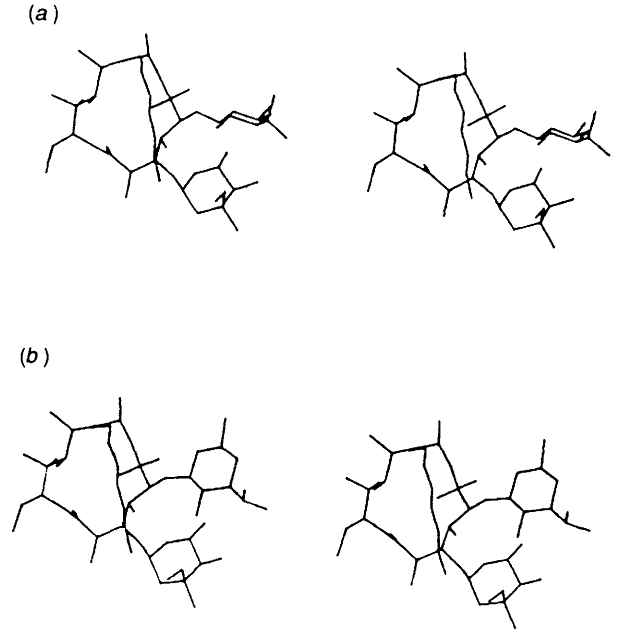

Fig. 12 *Protocol IV*. Stereoscopic views of the type **III** conformation. Protonated roxithromycin conformations **AaIII** (100 ps) and **AcIII** (80 ps). The appearance of this type **III** hydrogen bonding, 11-OH///O=C(1), is linked to the deformation of the macrocycle in the region C(9) to C(1). The modifications in this region [the C(11)–C(13) segment with a nearly all-*anti* zig-zag conformation] are due to the different orientations of the oxime chain, 11-OH and O=C(1). The reorientation of the lactone group C(1)=O, which folds inside the macrocycle, allows the 11-OH to form a hydrogen bond with C(1)=O. This region is rearranged according to the orientation of the C(1)=O group and the end of the oxime chain pushing back on the cladinose. (*a*) The **a** conformation is characterized by a desosamine orientation nearly perpendicular to the macrocycle and is differentiated in the **AaIII** (100 ps) conformation according to the type of hydrogen bond. (*b*) The **c** conformation corresponding to **AcIII** (80 ps) is characterized by a desosamine sugar coplanar to the macrocycle.

(*a*)

(*b*)

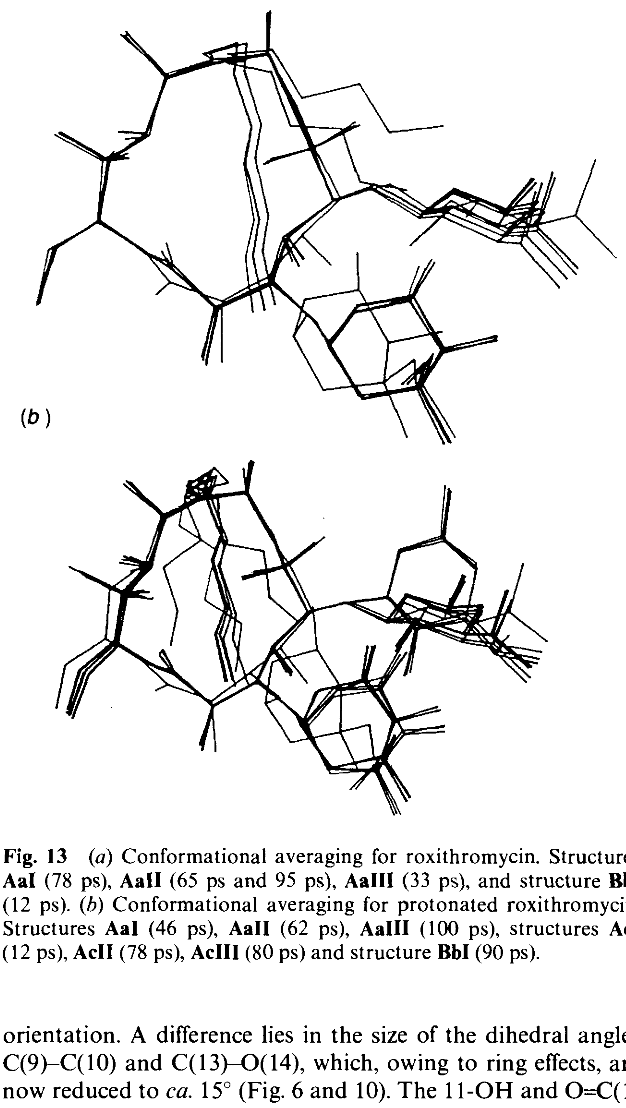

Fig. 13 (*a*) Conformational averaging for roxithromycin. Structures **AaI** (78 ps), **AaII** (65 ps and 95 ps), **AaIII** (33 ps), and structure **BbI** (12 ps). (*b*) Conformational averaging for protonated roxithromycin. Structures **AaI** (46 ps), **AaII** (62 ps), **AaIII** (100 ps), structures **AcI** (12 ps), **AcII** (78 ps), **AcIII** (80 ps) and structure **BbI** (90 ps).

lactone. The hydrophobic face of roxithromycin gives rise to more steric hindrance for all the methyl groups. Moreover, this provides better access to hydroxy protons on the other face to bind to the oxime chain by hydrogen bonding.

Hydrogen Bonding.—In roxithromycin, the NOE difference ^1H NMR spectrum arising from irradiation of the 6-OH proton, exhibits the NOE[6-OH]H(17) which results from an inter-residue hydrogen bond O(17)/////HO-6 between the oxime chain and the macrocycle. Similarly, 11-OH is found to be close in space to H(16) (NOE[11-OH]16). Hydroxy protons are excellent starting points for NOE experiments because, when the exchange processes that occur are sufficiently slowed down by intramolecular hydrogen bonding, their residence time, at any one position, is longer and, as a result, their saturation will have local effects.

Hydrogen-bond types are characterized as follows: X-ray: 6-OH///O(19), type **I**: 6-OH///O(16), type **II**: 6-OH///O(17), type **III**: 11-OH///O=C(1). These structures do not have the same number and location of minima.

It appears that intra-residue hydrogen bonding, such as type **III**, 11-OH///O=C(1), plays a role in determining the conformation of a large region [from C(9) to C(1)] of the antibiotic macrolide (Fig. 12). Recently,[11] a hydrogen bond between 11-OH and O=C(1) has been detected in the crystal structure of a 9-dihydroerythronolide B derivative. On comparing this last crystal structure **S** with the Perun model,[27] the similarity of both conformations, in particular the C(11)–C(13) segment with a nearly all-*anti* (zig-zag) conformation, can be detected. This bond can occur only when 11-OH and O=C(1) change their orientation. A difference lies in the size of the dihedral angles C(9)–C(10) and C(13)–O(14), which, owing to ring effects, are now reduced to *ca.* 15° (Fig. 6 and 10). The 11-OH and O=C(1) groups are close enough to form a hydrogn bond. The energies of these structures (**III**) increase by over 2–3 kcal. The orientation of the hydroxy group has a large effect on the potential energy and the location of each low-energy minimum. Roxithromycin probably exists in the form of two ring-conformers **AII** and **AIII** and, in $CDCl_3$, a hydrogen bridge is formed that lowers the barrier enough to make interconversion possible.

The main effect of the 6-OH position is on the structures **I** and **II**. Hydrogen bond **II** involving 6-OH///O(17) gives low-energy structures, but the energy is 'higher' in the corresponding **I** structures with 6-OH///O(16). The crystal structure shows an inter-residue hydrogen bond 6-OH///O(19) between the oxime chain and the macrocycle. When the O(19) is free, at 0 ps, and not involved in any hydrogen bonding, the oxime chain is anchored to the erythronolide by O(16) only [type **I**, 6-OH///O(16)], above the macrocycle, thereby giving rise to some of its mobility.

This position, induced by hydrogen bonding type **I**, increases the freedom of the macrocyclic lactone ring and consequently the degree of movement of the desosamine and the cladinose sugar in the following ways.

(i) Firstly movement of the macrocycle is relative to the C(2)–C(3)–C(4)–C(5) region (conformation **B**). H(3) proton folds inside the macrocycle, the cladinose lifts up again, above the macrocycle, and allows the desosamine to rotate slightly with respect to the macrocycle. This particular position **b** of the cladinose sugar repels the oxime chain on the right, which therefore moves beyond the unprotonated desosamine, close to its β face, with a characteristic spatial proximity between 19-OMe and 5′-Me (Fig. 8). However for the protonated derivative **2**, the $NH^+(Me)_2$ group hinders this approach near to the desosamine, so it pushes away the oxime chain on the left towards the carbonyl C(1)=O, with a characteristic spatial proximity between 19-Me and H(13) (Fig. 11).

(ii) Secondly movement induced by the raising of the oxime chain, is relative to the C(13)–O(14)–C(1)–C(2) region (conformation **S**). The reorientation of the lactone group C(1)=O, which folds inside the macrocycle, allows the 11-OH to form a hydrogen bond with C(1)=O (type **III**). This region is rearranged according to the orientation of the C(1)=O group with the end of the oxime chain pushed back on to the cladinose (Fig. 12).

However, when the oxime chain comes down towards the macrocycle again, with a new inter-residue hydrogen bond type **II** [O(17)/////HO-6], the different hydrogen bonding associations reduce the degree of freedom of the macrocyclic lactone ring (conformation **A** only) and consequently, the motion of the desosamine and cladinose sugar (conformation **a** only). In the **AaII** structure, the end of the oxime chain is situated above the H(3) and H(1″), close to the cladinose sugar. This sugar is thus pushed back onto the desosamine, which consequently loses some of its mobility, and the two α faces of the cladinose and the desosamine rings are opposite to each other (Fig. 8). It can thus be concluded that roxithromycin **1** is locked in an **AaII** globular form and this rigidification has consequences for the mobility of sugars.

However, if the molecule is protonated (**2**), the desosamine sugar undergoes an **a** $\Longleftrightarrow$ **c** interconversion to adopt a stable conformation **c**, with an orientation nearly coplanar with that of the macrocyclic lactone ring. Thus the cladinose sugar bound in C(3), adopts a conformation with an orientation nearly perpendicular to the macrocyclic lactone ring. In this **AcII** conformation (Fig. 11), the chain is orientated above the macrocyclic lactone ring and the O(17) is engaged in hydrogen bonding with the 6-OH group of the macrocycle, but with the 19-OMe and the carbonyl group, C(1)=O in close proximity.

In the same way for (**2**), two new intramolecular hydrogen bonds (involving the desosamine sugar) appear in 100% of the generated structures, 3′-$N(Me)_2H^+$///OH-2′ and 2′-OH///O(5). Perhaps these new hydrogen bonds formed lower the barrier enough to make interconversion **a** $\Longleftrightarrow$ **c** possible in compound **2**. A previous study has shown that roxithromycin is metabolized *in vivo* only into a complex absorbing at 455 nm, since some tissues have alkaline pH, and that the reactivity of the nitrogen atom of the *N*,*N*-dimethylamino group causes shifts to occur if the amine is protonated or if the concentration in the same solvent is changed. Furthermore, the magnitude of the shift depends on several factors including pH, the nature of the counterion and on the degree of hydrogen bonding.

Additional NMR studies on the presence of hydrogen bonds have been performed,[14] investigating concentration and temperature effects. They have demonstrated that 6-OH and 11-OH are implicated in inter-residue hydrogen bonding in roxithromycin to a greater extent than the other hydroxy groups. The oxygen O(16) and 17-OCH_2 and the nitrogen C(9)=N atoms are engaged in hydrogen bonding with the protons of two hydroxy groups from the macrocycle, 11-OH and 6-OH, and give rise to an intramolecular hydrogen-bond network in both the macrocycle and the oxime chain residues. It should be noted that hydrogen-bonding involving 6-OH and 11-OH has been implicated in tautomeric and conformational equilibria in erythromycin A.[28]

The different types of hydrogen bonding **I**, **II**, **III**, all appear to contribute to the isomerization of the low-energy conformers to produce a more stable solution conformation.

Conclusions

The computational methodologies presented illustrate the usefulness of MD in elucidating possible solution conformations starting with a crystal structure. The structural information (dihedral angles and spatial proximity) of the different conformations generated should be of great benefit in predicting the conformation in solution of a new roxithromycin derivative. At the same time, detailed examination of the NMR data generated from roxithromycin revealed that approximate solution structures can be estimated. From this we are able to postulate a reasonable solution structure for roxithromycin and its protonated analogues.

The desosamine sugar is flexible in **2** and gives rise to large amplitudes for the glycosidic angles corresponding to three different orientations (two essentially **a** and **c**), but not to large fluctuations in the total energy. MD shows conformational changes not only in the macrocyclic lactone (**A** and **B**) but also in the sugar rings (**a** and **c**). This result is not in agreement with previous studies on the other erythromycin A derivatives which show the same orientation of the sugar rings with respect to one another and with respect to the lactone ring.

Thus, it is clear from the above results that, in $CDCl_3$ at room temperature, interconversion (*i*) between conformations **Aa** and **Ac** and (*ii*) between conformation type **AII** and type **AIII**, is possible but interconversion of some type **A** and type **B** members is neither allowed nor observed (low ratio, high minimized energy, unstable). However, it was concluded for erythromycin A that a minor conformer **B** or **B′** was in equilibrium with a major one (X-ray crystal structure).

NMR parameters reflect the virtual conformation and suggest that a solution of roxithromycin is not adequately described by the crystal structure conformation. This study shows that these molecules are best described as a blend containing varying proportions of conformations **A** but less likely **B**. It has also been shown that the steric contribution of the oxime residue has an effect on the activation barrier for isomerization. Isomerizations are localized events and the transitions between energy minima probably involve concerted movements of many different portions of the molecule.

The use of MD simulations showed a series of coordinated movements, which are induced by the mobility of the oxime chain according to the hydrogen bonding; its lowering or raising allows conformational reorganization of the macrocycle, namely, folding relative to the C(3) portion (**A** $\Longleftrightarrow$ **B**) or to the C(1)=O group (**AII** $\Longleftrightarrow$ **AIII**). These movements themselves lead to rotation of glycosidic bonds correlated to the three original orientations of the sugar rings, **a**, **b** and **c**.

Experimental

The compound studied, experimental formula $C_{41}H_{76}N_2O_{15}\cdot H_2O$, is an antibiotic CID named roxithromycin, proprietary name Rulide M_R = 854.99 (RU 28965-11).[1] ^1H NMR experiments were conducted on Bruker WM250 (or AM400 or AM500) NMR spectrometers, using a sample concentration of 5×10^{-2} mol dm^{-3}. The samples were at ambient temperature (20 °C) unless otherwise noted and were degassed, in $CDCl_3$.

The 2D phase-sensitive ^1H NOESY experiment was performed with variation of the mixing time (D8) (D9 P2 A0).[29] FIDS were acquired (256 scans, two dummy scans) over 1275 Hz into a 1 K data block for 512 increments values of the evolution time, t_1. The raw data were zero filled to a 2 K × 2 K matrix and the first FID was divided by two. Different experiments in $CDCl_3$ and in CD_3OD were performed with τ_m = 0.2, 0.3 s and the relaxation delay D_1 was 1.5 s.

The ^{13}C T_1 experiment used an inversion–recovery pulse sequence with a relaxation delay D_1 = 4 s and averaging 2800 scans into a 8 K data block. The experiment was repeated for 15 values of VD ranging from 0.01 s to 3 s. The T_1 values were calculated using the Bruker DISNMR program. The 180° pulse had been calibrated and the value was 19 μs in $CDCl_3$ and in CD_3OD solution.

Measurements of long-range heteronuclear (^{13}C–^1H) coupling constants were performed on the WM250 spectrometer using 2D selective INEPT on a sample of 60 mg in 0.75 cm^3 of $CDCl_3$ in 5 mm NMR tubes. A selective 2D INEPT experiment[22–23] was performed using a version derived from the 1D A Bax experiment.[24] Here, the selective excitation of a proton signal allows detection of a single doublet for the corresponding (carbon(s). Selectivity was achieved by a DANTE pulse *via* the decoupler channel with 48 short pulses of 5 μs separated by a D2 delay of 0.5 ms. Selectivity was equal to $\Delta\nu$ $^1H \pm 21$ Hz ($\gamma B_1/2\pi \approx 21$ Hz).

The 90° non-selective proton pulses were 140 μs long. The relaxation delay was 1.4 s and each FID was acquired with 4800 scans with broad-band decoupling. 24 Experiments were carried out, then data were zero-filled to 128 points in the F1 dimension. In the F2 dimension, data were acquired with 4096 points; no zero-filling was applied. Resolution enhancement by Gaussian transformation was carried out in the F2 dimension.

The D0 delay, during which the carbon satellite doublets of the selected protons evolve, was increased by 0.01 s between each experiment. D0 was initially set to a value of 3×10^{-6} s. A preliminary set-up of the experiment was necessary to adjust the D3 delay, in order to avoid loss of ^{13}C signal due to relaxation and to optimize the detection of high-value coupling constants. D3 was thus set to 30 ms corresponding to $1/nJ_{CH}$ with $J_{CH} \approx 5$ Hz.

After double Fourier transform of the time-domain data, the resolution was 0.4 Hz and 3 Hz in F1(J_{CH}) and F2 (^{13}C chemical shifts) dimensions respectively. The total experimental time was 63 h. The spectral width was ± 25 Hz and 12 195 Hz in the F1 and F2 dimensions, respectively.

Molecular-dynamics and -mechanics Calculations.—A molecular-dynamics simulation was performed for roxithromycin (**1**) and protonated roxithromycin (**2**) using the 'DISCOVER' program from the Biosym package[16] on a Silicon-Graphics 4D-20G computer. The molecule was initially built from the X-ray crystal data of roxithromycin. Charges and atomic potentials were then redefined for the new molecule (**2**) using the built-in algorithm of the program.[17]

We used the CVFF forcefield from Dauber-Osguthorpe[16] in which cross-terms represent the coupling of the deformations of internal coordinates and describe the coupling between adjacent bonds. These terms are required accurately to reproduce experimental vibrational frequencies and therefore the dynamic properties of molecules. A Morse function was used to describe the stretching of bonds.

For the electrostatic energies, since no explicit solvent molecules were incorporated during the run, the relative permittivity was set distance-dependent (ε=R_{ij}), weighting more heavily short distance polarisation interactions and damping long ones, to mimic the solvent effect.[12] For the same reason, no periodic-boundary conditions were required. A cut-off function was applied for non-bonded interactions, decreasing their effect smoothly between 18 and 20 Å, avoiding discontinuity and shortening the computation time. The neighbour list was recomputed every 10 iterations.

Newton's equations of motion were integrated every femtosecond and the rescaling of the temperature was controlled by the Verlet algorithm. Too large a deviation from the target temperature is thus avoided.

The structure was first energy minimized using two different alorithms: steepest-descent for 100 iterations and then conjugate gradient until the first energy derivative was less than 0.1 kcal mol^{-1}.

A preliminary run was performed with a 4 ps equilibration period, in which the system was coupled to a thermal bath at 300 K to relieve strains in the structure and reach thermodynamic equilibrium. The simulation was then continued with an 8 ps period at 300 K followed by a temperature jump to 600 K for 4 ps. This alternation was repeated until a total simulation time of 40 ps was reached. Every ps, the simulation was stopped and the remaining structure was energy minimized using the previously described method. A second set of simulations was carried out without any temperature jumps at 300 K for 100 ps, with energy minimization each ps as above.

Acknowledgements

We thank Laboratoire Roussel (Paris) for their scientific and financial support during this research and we are grateful to Pr. Aliette Cossé, University Paris VII, for stimulating discussions and to Dr. Sian Miller for skilful assistance.

References

1 J. F. Chantot, J. C. Gasc, S. Goin D'Ambrieres and A. Lutz, *23rd Intersciences Conference on Antimicrobial Agents in Chemotherapy*, 1983, Abstract 447, Las Vegas (USA); J. F. Chantot, A. Bryskier and J. C. Gasc, *J. Antibiot.*, 1986 **39**, 660.
2 D. A. Pye, J. I. Gyi and J. Barber, *J. Chem. Soc., Chem. Commun.*, 1990, 1143.
3 E. G. Brain, A. K. Forrest, E. Hunt, C. Shillingford and J. M. Wilson, *J. Antibiot.*, 1989, **42**, 1817.
4 *Roxithromycin: a new macrolide*, Special issue of the Journal of Antimicrobial Chemotherapy, 1987, **20**, Suppl. B.
5 F. Kees, H. Grobecker, J. B. Fourtillan, D. Tremblay and B. Saint Salvi, *Brit. J. Clin. Pract.*, 1988, **55**, 51.
6 A. McLean, J. A. Sutton, J. Salmon and D. Chatelet, *Brit. J. Clin. Pract.*, 1988, **55**, 52.
7 M. Delaforge, E. Sartori and D. Mansuy, *Chem. Biol. Inter.*, 1988, **68**, 179.
8 J. Gharbi-Benarous, M. Delaforge, I. Artaud and J. P. Girault, *Magn. Reson. Chem.*, 1990, **28**, 846.
9 J. R. Everett and J. W. Tyler, *J. Chem. Soc., Perkin Trans. 2*, 1986, 1659; 1988, 325; J. R. Everett and J. W. Tyler, *J. Chem. Soc., Chem. Commun.*, 1987, 815; J. R. Everett and J. W. Tyler, *Magn. Reson. Chem.*, 1988, **26**, 179.
10 J. R. Everett, I. K. Hatton, E. Hunt, J. W. Tyler and D. J. Williams, *J. Chem. Soc., Perkin Trans. 2*, 1989, 1719; J. S. Davies, J. R. Everett, I. K. Hatton, E. Hunt, J. W. Tyler, I. I. Zomaya, A. M. Z. Slawin and D. J. Williams, *J. Chem. Soc., Perkin Trans. 2*, 1991, 201.
11 J. Mulzer, H. M. Kirstein, J. Buschmann, C. Lehmann and P. Luger, *J. Am. Chem. Soc.*, 1991, **113**, 910.
12 P. Kollmann, *J. Am. Chem. Soc.*, 1984, **106**, 765.
13 C. Manuel, P. Delamonica, M. J. Rosset, C. Safran, D. Pirot, L. Audegond and J. C. Pechere, *16th International Congress of Chemotherapy*, 1989, Abstract 1224, Jerusalem; B. J. Luft and J. S. Remington, *J. Infect. Dis.*, 1988, **157**, 1; G. A. Dette, *Infection*, 1979, **7**, 129; W. E. Wellman, H. W. Dodge, F. R. Heilman and M. C. Petersen, *J. Lab. Med.*, 1954, **43**, 275; J. M. Hofflin and J. S. Remington, *Antimicrob. Agents and Chemother.*, 1987, **31**, 346; H. R. Chang and J. C. Pechere, *Antimicrob. Agents and Chemother.*, 1987, **31**, 1147.
14 J. Gharbi-Benarous, M. Delaforge, C. K. Jankowski and J. P. Girault, *J. Med. Chem.*, 1991, **34**, 1117.
15 B. Bachet, C. Brassy and J. Mornon, *Acta Crystallogr., Sect. C*, 1988, **44**, 112.
16 P. Dauber-Osguthorpe, V. A. Roberts, D. J. Osguthorpe, J. Wolff, M. Genest and A. T. Hagler, *Proteins: Structure, Function and Genetics*, 1988, **4**, 31.
17 U. Dinur and A. T. Hagler, *J. Chem. Phys.*, 1989, **91**, 2949.
18 H. J. C. Berendsen, J. P. M. Postma, W. F. van Gunsteren, A. DiNola and J. R. Haak, *J. Chem. Phys.*, 1984, **81**, 3684.
19 A. Nakagawa and S. Omura, *Macrolide Antibiotics. Chemistry, Biology, and Practice*, Ed. S. Omura, Academic Press, Orlando, 1984, 75.
20 I. Tvaroska, M. Hricovini and E. Petrakova, *Carbohydr. Res.*, 1989, **189**, 359.

21 M. Karplus, *J. Am. Chem. Soc.*, 1963, **85**, 2870; L. P. Durette and D. Horton, *Org. Magn. Reson.*, 1971, **3**, 417; G. Vorontsova and A. F. Bochkow, *Org. Magn. Reson.*, 1974, **6**, 654; J. Gharbi-Benarous, G. Dana, M. Philoche-Levisalles and C. Bois, *Magn. Reson. Chem.*, 1988, **26**, 457; S. G. Bratsch, *J. Chem. Educ.*, 1985, **62**, 101.
22 T. Jippo, O. Kamo and K. Nagayama, *J. Magn. Res.*, 1986, **66**, 344.
23 M. Hricovini, I. Tvaroska, D. Hurin and G. Y. Batta, *J Carbohydr. Chem.*, 1989, **8** 389.
24 (*a*) A. Bax, *J. Magn. Reson.*, 1984, **57**, 314; (*b*) H. Kessler, U. Anders and G. Gemmecker, *J. Magn. Reson.*, 1988, **78**, 382; W. Bermel, K. Wagner and C. Griesinger, *J. Magn. Reson.*, 1989, **83**, 223; M. Ochs and S. Berger, *Magn. Reson. Chem.*, 1990, **28**, 994; (*c*) G. A. Morris and R. Freeman, *J. Magn. Reson.*, 1978, **29**, 433; (*d*) Michael J. Gidley and Stephen M. Bocick, *J. Chem. Soc., Chem. Commun.*, 1985, 220.
25 A. A. van Beuzekom, F. A. A. M. de Leeuw and C. Altona, *Magn. Reson. Chem.*, 1990, **28**, 68.
26 D. Marion and K. Withrich, *Biochem. Biophys. Res. Commun.*, 1983, **113**, 976.
27 R. S. Egan, T. J. Perun, J. R. Margin and L. A. Mitscher, *Tetrahedron*, 1973, **29**, 2525; T. J. Perun, R. S. Egan and J. R. Martin, *Tetrahedron Lett.*, 1969, 4501.
28 J. R. Everett, E. Hunt and J. W. Tyler, *J. Chem. Soc., Perkin Trans. 2*, 1991, 1481.
29 P. H. Bolton and T. L. James, *J. Am. Chem. Soc.*, 1980, **102**, 1449; M. A. Delsuc, Thèse d'Etat, 1985, University Paris-11.

Paper 2/01274J
Received 9*th March* 1992
Accepted 27*th April* 1992